ELSEVIER

Quaternary Science Reviews 23 (2004) 335–357

QSR

The climate of the Earth at Last Glacial Maximum: statistical equilibrium state and a mode of internal variability

W.R. Peltier[a,*], L.P. Solheim[b]

[a] *Department of Physics, University of Toronto, 60 St. George Street, Toronto, Ont., M5S 1A7 Canada*

[b] *Canadian Climate Centre for Modelling and Analysis (CCCma), University of Victoria, Victoria, BC, V8W 3P6 Canada*

Received 8 April 2003; accepted 13 July 2003

Abstract

We report the results obtained for the climate of the Earth at Last Glacial Maximum based upon multi-millennium integrations of a model of the coupled atmosphere–ocean–sea ice–land surface processes, system. The model employed is the low spatial resolution (T31) paleoclimate version of the Community Climate System Model that has been developed at the National Center for Atmospheric Research (NCAR) with important input from the UCAR community. In this initial discussion of the results delivered by the model for LGM, we focus upon the primary characteristics of the statistical equilibrium state of both atmosphere and ocean. Also discussed are the characteristics of the ENSO mode of internal climate variability that the model predicts to obtain under glacial conditions. Our analysis suggests that the degree of tropical cooling at LGM is approximately 4.5°C over the equatorial Pacific sector, a value that is somewhat higher than has been obtained in other recent simulations of LGM climate. We also find that the strength of the ENSO phenomenon is significantly increased at LGM relative to its expression in the modern climate system. In order to achieve a statistical equilibrium representation of LGM climate, we have been obliged to integrate the coupled system for over 2000 years, a fact that has important implications for snapshot analyses of paleoclimatic state when a coupled atmosphere–ocean model is employed.

1. Introduction

During the quarter century that has passed since completion of the CLIMAP (1976, 1981, 1984) project, there have been numerous attempts to employ coupled atmosphere–ocean models of the climate system to infer the properties of the surface climate of the Earth that must have obtained at Last Glacial Maximum (LGM), approximately 21,000 calendar years before present (BP). This seminal project produced two primary data sets, namely those for the geographical locations and thicknesses of the continental ice-sheets that were then in place, and for the variations of sea surface temperature (SST) that were characteristic of the LGM state. The former data set provided a means by which one could represent the first-order changes in surface topography and continental albedo that are required surface boundary conditions for the reconstruction of surface climate using a modern Global Climate Model (GCM). The latter data set for SSTs has been employed either to fix the temperature boundary condition over the oceans for the purpose of fixed SST reconstructions of surface climate, or as a means of validating the predictions of models that include a means of directly computing the changes in SSTs expected in consequence of the changes in orbital insolation forcing, atmosphere CO_2 and other trace gas concentrations, and surface topography and albedo, that were characteristic of LGM conditions.

Most of the coupled atmosphere–ocean models that have been employed to predict the change in SSTs have employed simple mixed layer models of the oceans with heat fluxes in the mixed layer tuned to enable the models to provide an acceptable fit to the observed annual cycles of SSTs and sea ice extent that obtain under modern climate conditions. In the context of the Paleoclimate Model Intercomparison Project (PMIP), the predictions of a large number of such models have recently been intercompared (e.g. see Pinot et al., 1999;

*Corresponding author. Tel.: +1-416-978-2938; fax: +1-416-978-8905.

E-mail address: peltier@atmosp.physics.utoronto.ca (W.R. Peltier).

0277-3791/$ - see front matter © 2003 Elsevier Ltd. All rights reserved.
doi:10.1016/j.quascirev.2003.07.003

Vettoretti et al., 2000), the primary result being the demonstration of the extremely large discrepancies that exist between the predictions of these models for surface temperatures on both land and sea in both the tropics and the extra-tropics. In Fig. 2 of Vettoretti et al. (2000), for example, it is shown that the predicted depression of SSTs within the tropical belt varies from a low of −3.8°C the second generation Canadian Climate Centre model, CCC2 to a high of −0.8°C (the UGAMP model). All of the analyses of LGM climate performed in the context of PMIP employed the paleotopography and land–sea–ice mask of Peltier (1994, 1996) to fix these surface boundary conditions, implying that variations in these boundary conditions could not be the cause of the discrepancies in surface temperature predictions. Although the UGAMP result is broadly consistent with the original result of the CLIMAP project, the CCC2 result concerning the degree of tropical cooling is much larger than this earliest inference. Further discussions of results for the tropical cooling of SST in LGM climate will be found in IPCC (2001).

Now the CLIMAP inferences of SST were derived through application of the transfer function methodology based upon species abundances of foraminifera that had been developed by Imbrie and Kipp (1971), and since that time a variety of other proxies for SST determination have been developed, all of which seem to suggest that tropical SSTs were significantly colder than those obtained by the CLIMAP group. In particular, the alkenone proxy typically delivers estimates of the LGM SST depression in the tropics of 2–2.5°C (e.g. see Bard et al., 1997). The proxy based upon measurements of oxygen isotopes in corals, on the other hand, has delivered inferences in the range of 5°C (e.g. Guildersen et al., 2001). The further study by Lea et al. (2000) has suggested that tropical Pacific SSTs were at least 3°C colder than present. More recently, application of the Mg/Ca ratio proxy for SST, measured in the shells of foraminifera, has suggested that the temperature depression in the Pacific warm pool was in the range of 3.5–4.0°C (Visser et al., 2003). Because the surface temperature of the tropical ocean plays such an important role in the functioning of the climate system, this very large range of existing possibilities is extremely unsatisfactory.

In the process of attempting to reduce the uncertainties associated with our understanding of the LGM state of the climate system, much more complete models of this system than those employed in the context of the PMIP exercise are currently being applied. In particular, there have recently been a number of applications of complete coupled atmosphere–ocean–sea ice–land surface process models. The analysis by Bush and Philander (1998) was apparently the first in what has become a continuing sequence of such applications. In their attempt to assess LGM climate, the GFDL coupled model was employed and a single decade of integration was computed, again using as input the LGM paleotopography and land–sea–ice mask of Peltier (1994, 1996). The model was spun-up from an initial condition in which the oceans were in a state of no motion and the main result obtained was that tropical SSTs were found to be depressed by an amount between 4°C and 5°C (see Fig. 7 of Peltier and Solheim 2001 on which the Bush and Philander results are reproduced). This result has met with some skepticism due to the fact that the deep circulation of the oceans could not have played any role in determining the equilibrium state of the climate system in this analysis, as the time required in order for this component of the system to equilibrate is on the order of millennia. It is of course a legitimate question as to the role that this component of the ocean circulation would be expected to play in determining tropical SSTs.

A recent attempt to correct this possible flaw in the Bush and Philander analysis is that by Hewitt et al. (2001) who employed the HADCM3 model of the UK Hadley Centre, a fully coupled atmosphere–ocean model, to integrate the LGM climate towards a statistical equilibrium state for both the atmosphere and the oceans. The LGM integration once more employed the topography and land–sea–ice mask of Peltier (1994, 1996) to define the surface boundary conditions and after 700 years of integration, the model had yet to reach statistical equilibrium. Their analysis was, however, focused upon an attempt to determine the strength of the Atlantic thermohaline circulation under LGM conditions and they concluded that this circulation was significantly stronger at LGM than it is under modern conditions. An extension of this work has more recently appeared in Hewitt et al. (2003) in which the integration was continued to 1000 years. Again the primary result, shown in their Fig. 1, is that the LGM Atlantic THC is expected to have been stronger than modern. This result is sharply discordant with all currently available paleoceanographic proxies of the strength of North Atlantic Deep Water (NADW) formation under LGM conditions which strongly suggest that the deep circulation must have been considerably weaker at LGM rather than stronger (detailed discussion of this fact will be provided in what follows). It seems also to be the case that the HADCM3 atmospheric model is close to that of the UGAMP model which delivered the weakest equatorial cooling response of any of the models employed in the PMIP LGM tests in which the atmospheric models were coupled to mixed layer models of the oceans. It seems reasonable, then, to conclude this brief initial review of our model-based understanding of the LGM climate state, by saying that there continues to exist no concensus as to its primary characteristics, even when all models are employing the same surface

boundary conditions and the same solar radiation forcing.

The purpose of this paper is to contribute to the continuing debate concerning LGM climate by employing a different model of the coupled atmosphere–ocean system to study the nature of the equilibrium climate that should exist under LGM conditions. The model we will employ is the Community Climate System Model (CCSM) of the National Center for Atmospheric Research (NCAR), in particular the low (T31) resolution atmosphere and $3^\circ \times 3^\circ$ ocean model to which the atmosphere is coupled, in the version of this model that has been configured especially for paleoclimate analyses. The specific flavour of this paleoclimate capable model is that recently described in some detail by Otto-Bliesner and Bradey (2001) in which the diffusivities for heat and salt in the ocean were reduced globally, and the momentum diffusivity reduced and horizontal resolution increased in the equatorial ocean so as to enable the model to deliver an excellent facsimile of the ENSO phenomenon (see Meehl and Arblaster, 1998; Meehl et al., 2001 for a discussion of the modifications to the model that are required to obtain a good simulation of the ENSO phenomenon under modern climate conditions). Adequately resolving this process could conceivably significantly impact the mean surface temperature of the equatorial ocean under LGM conditions.

In the following section of this paper we will describe the design of the numerical experiments that have been performed to investigate the nature of the climate state that should have existed under LGM conditions. Section 3 presents the main results that have been obtained from the very long fully coupled integrations of the CCSM model that we have performed. The results we will describe herein pertain primarily to the properties of the LGM oceans rather than to the LGM atmospheric circulation. This focus is consistent with the issues we have elected to highlight in the Introduction to this paper. Conclusions are offered in Section 4 of the paper where we will also review remaining issues.

2. Design of the LGM climate reconstruction using the NCAR CCSM and the spin-up to equilibrium of the LGM and modern control models

In attempting to produce an a priori reconstruction of planetary climate at any time in the past, there are a number of modifications that must be made to a model that has been tuned so as to enable it to deliver a good facsimile of modern climate. The changes we have made to the CCSM for this purpose are the following:

(I) We have modified the planetary topography with respect to sea level so as to incorporate the influence of the great polar ice-sheets that were then in place upon the Northern Hemisphere continents near the rotation pole (these are illustrated in Fig. 1). This topography (including the land–sea–ice mask) is that of the ICE-4G (VM2) model of Peltier (1994, 1996) but includes the correction due to the action of "implicit ice" as discussed in Peltier (1998). This model of LGM paleotopography, which embodies an eustatic sea level fall of approximately 120 m, is currently under revision to incorporate the additional constraints discussed in Peltier (2002c). The new model, called ICE-5G (VM2), is described in Peltier (2003a) and is characterized by a eustatic fall of approximately 130 m. We will describe elsewhere the impact upon the atmospheric general circulation of the new surface topography boundary conditions. The impact upon the state of the oceans which is to be the focus in this paper is expected to be modest. The recently published analysis of LGM climate by Shin et al. (2003) has employed the original ICE-4G (VM2) paleotopography without correction for "implicit ice" and assumed a uniform 105 m depression of sea level to compute shelf exposure. This approach is inaccurate. The Shin et al. analyses will be discussed further in what follows.

(II) We have also modified the seasonal variation of solar insolation at the top of the atmosphere due to the changes in the eccentricity and obliquity of the orbit that existed 21,000 years ago at LGM. Fig. 2 shows the modern insolation distribution as well as the deviation from it that was characteristic of LGM. Inspection of the results shown on this figure demonstrates that the LGM insolation regime was not dramatically different than present.

(III) Also adjusted were the atmospheric concentrations of the primary radiatively active trace gases, namely CO_2, CH_4 and N_2O. The LGM concentrations of these gases were fixed to those inferred on the basis of measurements made on air bubbles in the ice of the Vostock ice-core (e.g. Petit et al., 1999). Specifically, these concentrations were taken to be 200 ppmv for CO_2, 400 ppbv for CH_4 and 275 ppbv for N_2O. In contrast, our control integration will be taken to be the climate state of the model for ca. 1950 when the greenhouse gas concentrations are assumed to have been 355 ppmv for CO_2, 1714 ppbv for CH_4 and 311 ppbv for N_2O. The control model is therefore NOT preindustrial. No attempt was made to incorporate the influence of atmospheric aerosols in the LGM integration although the concentration of terrigenous dust is known to have been high (e.g. see Reader et al., 2000). A future

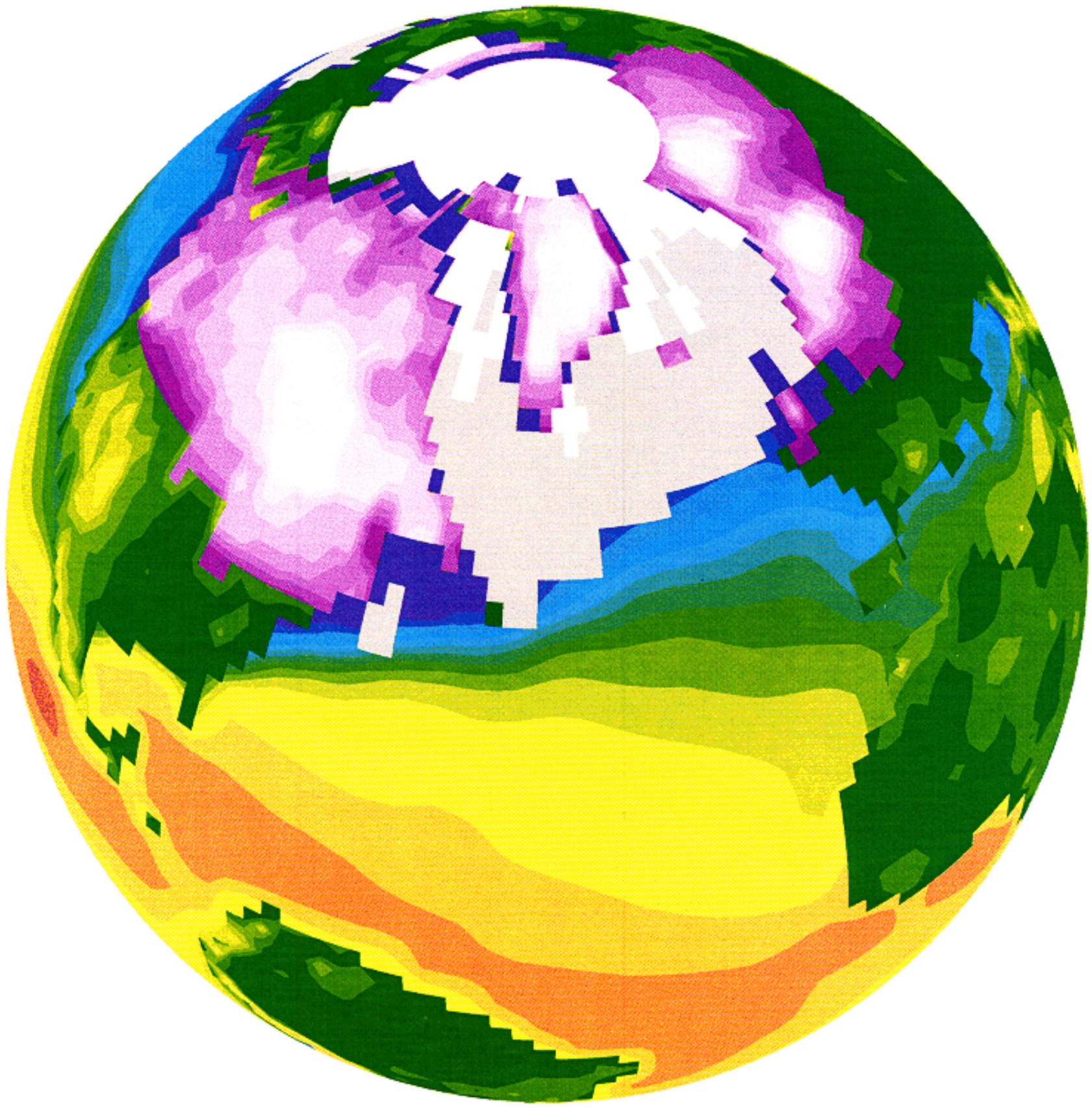

Fig. 1. Northern Hemisphere perspective views of the distribution of the great continental ice-sheets that were in place at LGM approximately 21,000 years before resent according to the ICE-4G reconstruction of Peltier (1994, 1996). The surface of the oceans in this graphic are coloured so as to represent the variation of annually averaged SST and so as to represent the winter and summer distributions of sea ice.

sensitivity analysis is planned to investigate the possible importance of this further influence upon LGM climate.

The results of the experiments that we will discuss herein will be based upon a comparison of those derived from a control model integration in which the ENSO resolving version of the CCSM is integrated to statistical equilibrium, and those derived from an LGM integration in which the model is modified as discussed above and which is also integrated to statistical equilibrium. Since the control model may be somewhat biased compared to modern climate, as to our knowledge, the ENSO resolving version of the CCSM has not previously been integrated to statistical equilibrium, our analyses will primarily be based upon a model–model intercomparison rather than upon comparison of the LGM integration to modern observations as in Peltier and Solheim (2002) in which results obtained following the first 1000 years of spin-up were compared in this way (more on this below).

Fig. 3 shows results for the spin-up to equilibrium of both the modern control integration and the LGM integration. As will be immediately evident by inspection of these results, the period over which the two models have been integrated is approximately 2000 years. It is important to realize that fully coupled integrations of the kind under discussion here have never before been produced at the relatively high spatial and temporal resolution being employed in this work using a model in which the application of "flux corrections" is unnecessary and in which the ENSO process is fully resolved (the very recently published results of Shin et al., 2003 obtained using the same model as we employ but a different spin-up procedure will be fully discussed in what follows). Results are shown in Fig. 3 for four different model characteristics during the spin-up phase of the integrations and for both the modern control and LGM simulations. Considering first the results for annually averaged surface air temperature, it will be noted that the control integration begins at a mean surface air temperature

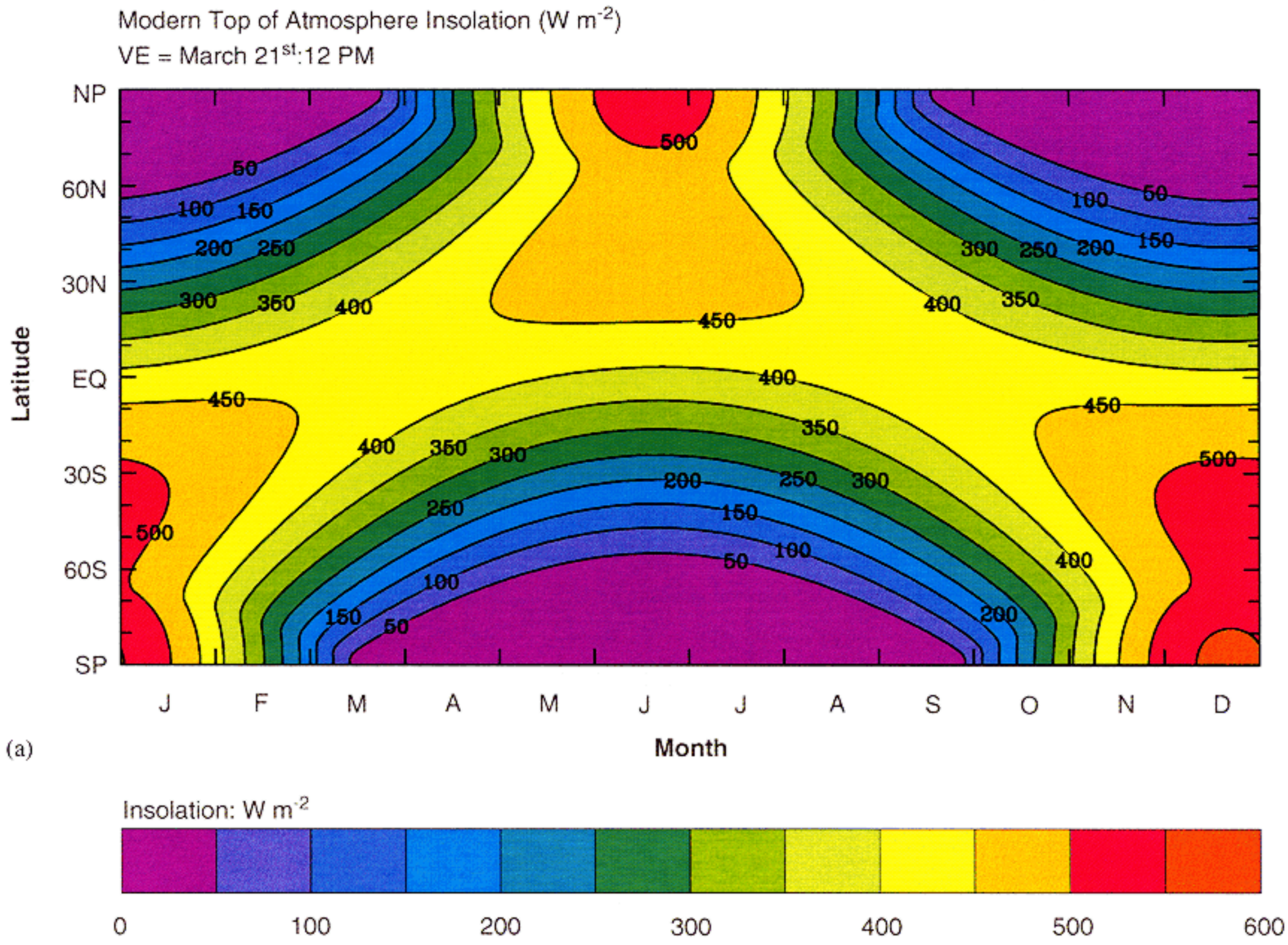

Fig. 2. Variation of insolation at the top of the atmosphere under modern climate conditions as well as the difference between this modern distribution and the distribution that existed at LGM.

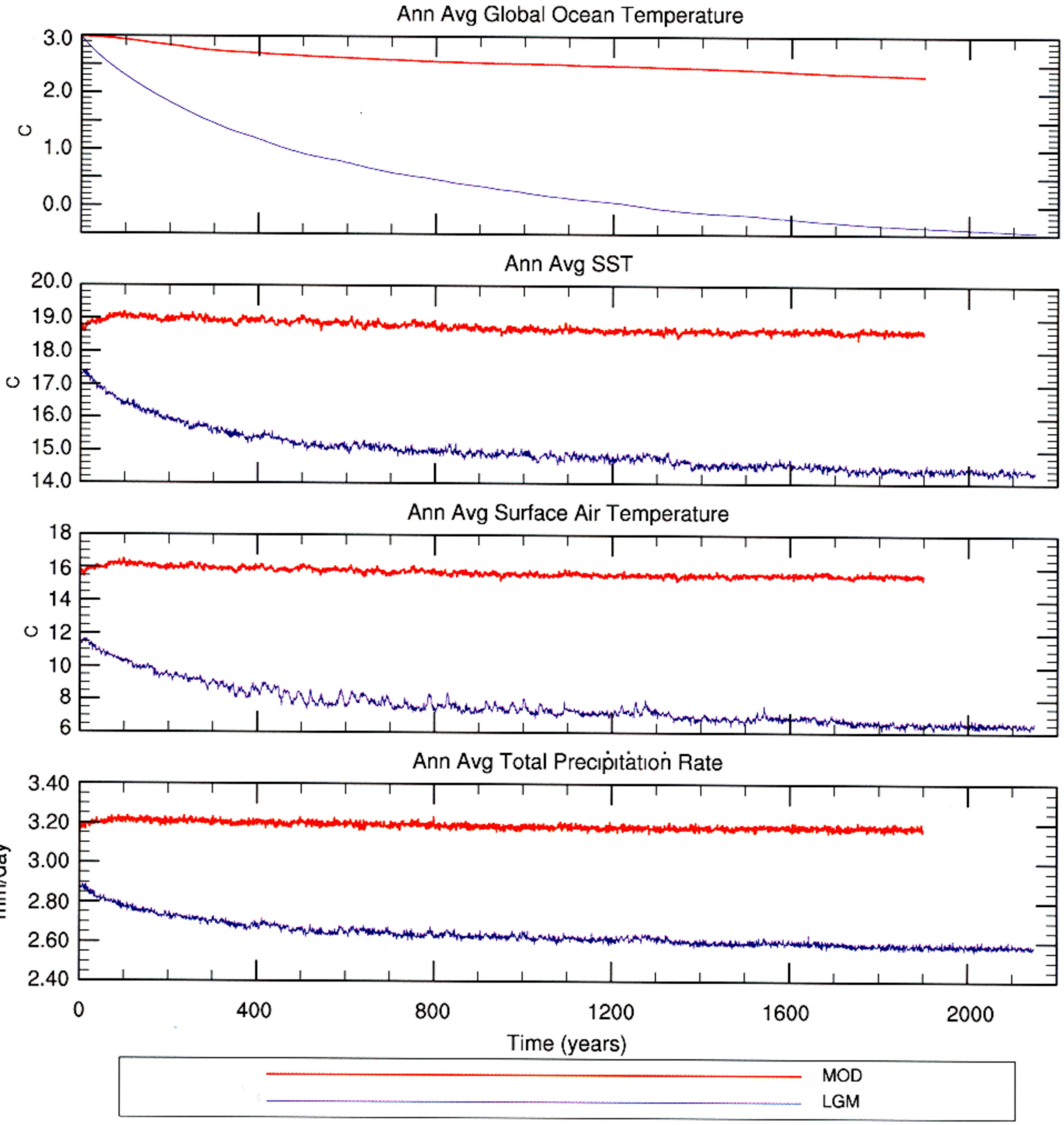

Fig. 3. Spin-up to equilibrium of the modern control integration and the LGM integration expressed in terms of several different global measures of climate evolution, measures described above the individual frames comparing the modern and LGM integration time series.

that is slightly in excess of 15°C and is essentially in statistical equilibrium initially. In comparison, the mean surface air temperature in the LGM integration is initialized from a state in which this temperature is somewhat less than 12°C. This initial condition was taken from the analysis reported in Peltier and Solheim (2001), in particular we employed the final state represented by curve 6 in Fig. 4 of that paper which was based upon a relatively short integration of the paleoclimate version of the CCSM that does not resolve ENSO. After initialization with these fields, the annually averaged surface air temperature in the LGM integration continues to drop significantly and eventually equilibrates at a level near 6.5°C. After the 2150 years of integration for which results are shown, it appears that statistical equilibrium of this characteristic of the climate at LGM has been essentially achieved. The difference in the mean surface air temperature of these two equilibria is therefore approximately 9°C.

Turning next to consideration of the annually and globally averaged SST in the model, it will be clear by inspection of the appropriate frame in Fig. 3 of this

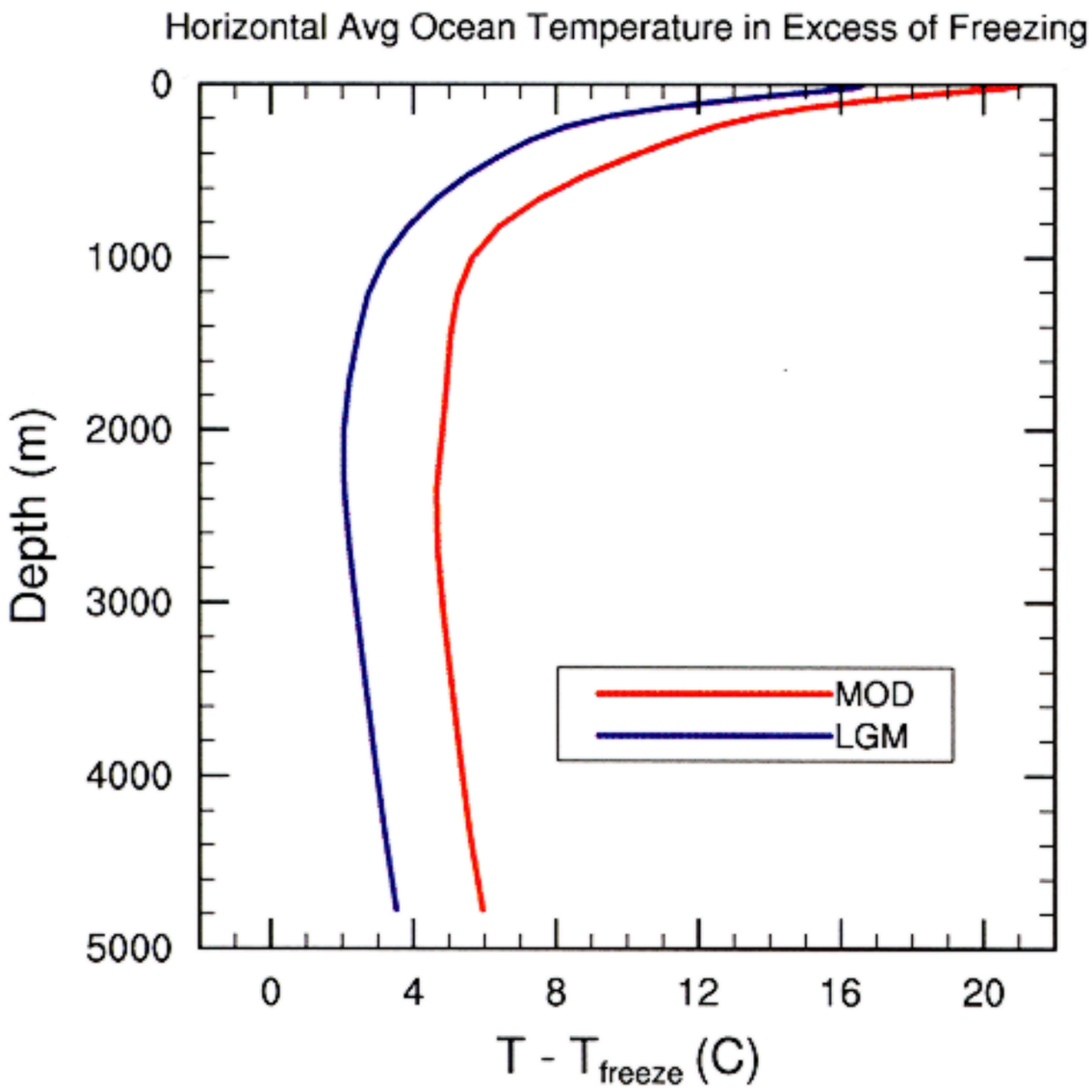

Fig. 4. Variation with depth of the horizontally averaged temperature of the global ocean from both the modern control and LGM integrations, expressed as the difference between the actual temperature and the depth dependent temperature at which the water would freeze.

paper that both the control and LGM integrations have also reached statistical equilibrium in terms of this quantity (in all of the analyses to be reported herein we take a state of statistically equilibrium to be fully established for a given field variable when the time derivative of this field has zero mean value when computed over the final 100 years of the simulation). The annually and globally averaged SST in the control and LGM simulations are respectively near 18.5°C and 14.5°C, implying a drop in the mean of approximately 4°C. The difference between the drop of mean annual surface air temperature of approximately 9°C and the drop of mean annual SST is a consequence primarily of the marked cooling that occurs over the continents, especially in those regions that are covered by the LGM ice sheets. Also shown in Fig. 3 are the spin-up results for the annually and globally averaged precipitation rate. Inspection of these data will show that, in statistical equilibrium, the control integration is characterized by a rate near 3.2 mm/day, whereas the equivalent result from the LGM integration is near 2.6 mm/day, a drop of approximately 19% and an entirely expected consequence of the reduced moisture holding capacity of the colder LGM air.

Of greatest interest in Fig. 3, however, are the spin-up results for the annually averaged global ocean temperature. Inspection of the data shown on the first plate of the figure, for both the control and LGM integrations, demonstrates that although both simulations are very close to statistical equilibrium in terms of this model characteristic after 1900 years of integration of the control model, and after 2150 years of integration for the LGM model, there remains some continuing, though small, secular cooling occurring (these integrations will be extended in future in order to examine the issue as to whether there may be some residual climate drift in these non-flux-corrected integrations of the CCSM). At the end of these integrations, the difference in the volume and annually averaged ocean temperature that has developed is 2.8°C with the control integration characterized by a temperature of approximately 2.3°C and the LGM integration by a temperature of approximately −0.5°C. It is important to realize that the latter result does not imply that the oceans should be frozen. To make this clear, Fig. 4 shows the variation with depth of the horizontally averaged temperature of the entire global ocean for both the control and LGM integrations at statistical equilibrium. These vertical profiles are presented as temperature relative to the freezing point according to the usually employed equation of state for sea water (e.g. Millero, 1978). Inspection of this figure demonstrates that, even in the glacial ocean, the temperature is not expected to fall much below 2°C above the freezing point.

Given that we have successfully integrated an ENSO resolving model of climate system evolution, which does not require flux corrections, into a state very close to statistical equilibrium, under both modern and LGM boundary conditions, we are in a good position to enquire as to the primary differences in the climate of the Earth between these two temporal epochs according to this model. Examples of these differences are discussed in what follows.

3. Results: the climate of the Earth at LGM; the mean state of the oceans and a primary mode of interannual variability

The data sets generated by the extended integrations of the ENSO resolving model will obviously be extremely useful for the analysis of a wide range of distinct climate system processes. For example, preliminary analyses of the first kyr of integration of the LGM run has already enabled us (Peltier and Solheim, 2002) to provide initial comment on the nature of the North Atlantic Oscillation in the model and to comment briefly upon ENSO itself. Of great interest will also be the exploration of the Pacific North America teleconnection pattern under glacial conditions, and the analysis of the interconnection between ENSO and the monsoon circulations. Here we will content ourselves with a discussion of the mean state of the oceans and of the nature of the ENSO process under glacial as opposed to modern conditions. These aspects of the

climate system are considered in the following two subsections.

3.1. The state of the glacial ocean at LGM

Focusing first upon the characteristics of the glacial ocean at LGM, it is important at the outset to add a caveat to the results we will present. It should be clear that the mean state of the LGM ocean, insofar as salinity is concerned, should be more saline than the modern ocean since the extraction of the freshwater required to build the LGM continental ice sheets would have increased mean salinity by approximately 3%. This is based upon the fact that eustatic sea level was lower at LGM by approximately 130 m (e.g. see Peltier 2002a, b for recent discussions). In designing the LGM experiment that will be discussed herein, however, we have elected to keep the mean salinity of the oceans fixed to the modern value of $\sim$ 35‰. Our intention in future work is to investigate the impact of the change in mean salinity that actually occurred (e.g. see Adkins et al., 2002) by spinning off a repeat LGM integration in which the appropriate mean increase in salinity is introduced. Given the sensitive dependence of the density of sea water upon salinity at low temperature, it is unclear on a priori grounds as to the impact that this influence will have upon the ocean general circulation and thereby upon climate. An initial analysis by Weaver et al. (1998), however, suggests this to be a small effect. Concerning the evolution of the mean salinity of the oceans over the course of the 2 millennium timescale of the control and LGM integrations however, it is important to note that the model does not precisely conserve this quantity. Fig. 5 illustrates the temporal evolution of this quantity for the two calculations, inspection of which will show that the mean salinity increases by somewhat less than a third of a percent over the course of each model run. As discussed in Boville and Gent (1998), the NCAR CCSM attempts to ensure conservation of freshwater by computing the area average of precipitation $\langle P \rangle$ and evaporation $\langle E \rangle$ over the "active" area of the oceans and then multiplying the precipitation over this region by the ratio $\langle E \rangle / \langle P \rangle$. This is done to compensate for the fact that the version of the model we are using has no river routing scheme. The result shown in Fig. 5 is important as it demonstrates that this version of the model does not conserve freshwater. It is conceivable that the slow continued cooling of global ocean temperature evident in the first plate of Fig. 3 could be associated with climate drift due to the weak secular variation of the mean salinity of the oceans. This must remain as a caveat on several of the results to be discussed in what follows.

The first property of the ocean upon which we wish to comment explicitly concerns the degree to which the

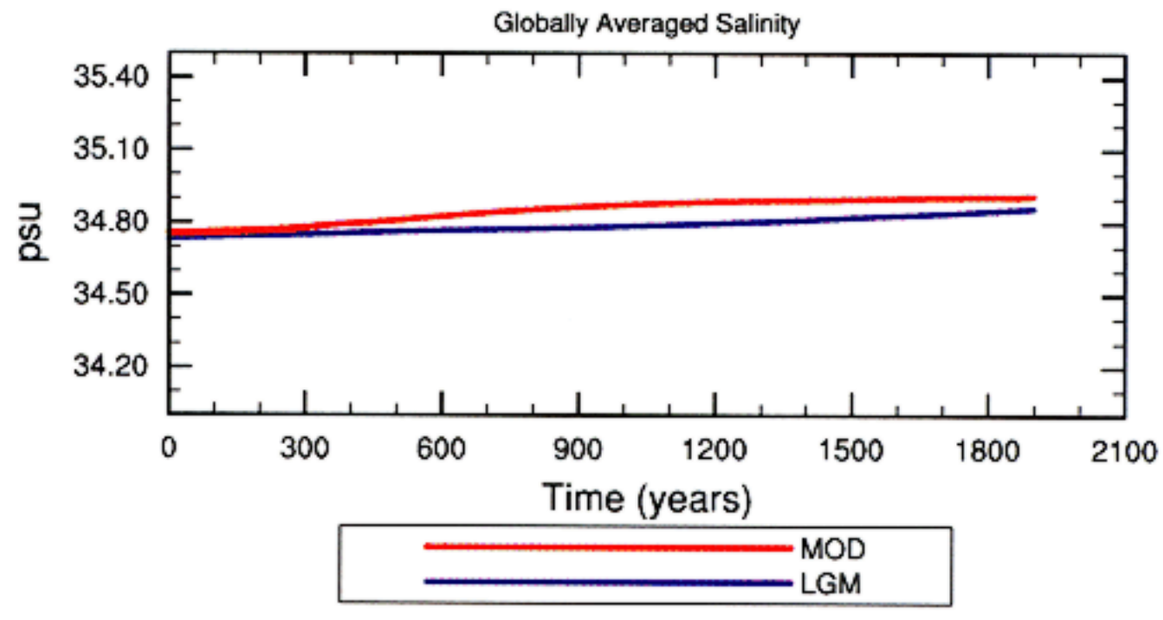

Fig. 5. Variation with time of the mean salinity of the oceans for both the modern control model and for the model of LGM climate.

abyssal waters in the individual ocean basins were cooled at LGM. To this end we show in Figs. 6 and 7 the spin-up to equilibrium of the deep water temperatures in each of the major ocean basins for the modern and LGM integrations respectively. Intercomparison of the results shown in these figures will demonstrate that the temperature of the deep water in the Atlantic Basin under modern conditions is expected to average to a value of approximately 0.25°C whether the vertical averaging is performed over the lower 500 m or over the lower 1800 m. The equivalent LGM predictions in Fig. 7 are characterized by bottom water temperatures near -2°C, with Pacific abyssal water being somewhat warmer than Atlantic abyssal water and the results once more being independent of the depth range over which the average is taken. These results for the LGM oceans are quite compatible with the most recent inferences of temperature of abyssal waters based upon measurements in pore waters of LGM age extracted from deep sea sedimentary cores (Adkins et al., 2002; see also the comments by Boyle, 2002). The results of Adkins et al., based upon measurements made on single hydraulic piston cores raised from the Atlantic, Antarctic and Pacific basins, give inferences of LGM deep water temperatures of -1.5 ± 0.5°C, -1.2 ± 0.5°C and -1.3 ± 1.0°C respectively. It will be noted that our values, although generally within the authors stated uncertainties, are on the cool side of the measurements themselves. It is conceivable that these offsets could be associated with the climate drift mentioned above.

Of greater interest insofar as the present paper is concerned is the impact upon the Atlantic thermohaline circulation of the change in boundary conditions from those appropriate to modern conditions to those characteristic of LGM. This intercomparison is shown in Fig. 8 where we present the meridional transport stream function (MTSF) for the Atlantic basin between 30° south latitude and the north pole. Very clear by inspection of this figure is the marked reduction in the strength of the cell that is driven by the formation of NADW and the simultaneous reduction in the depth to

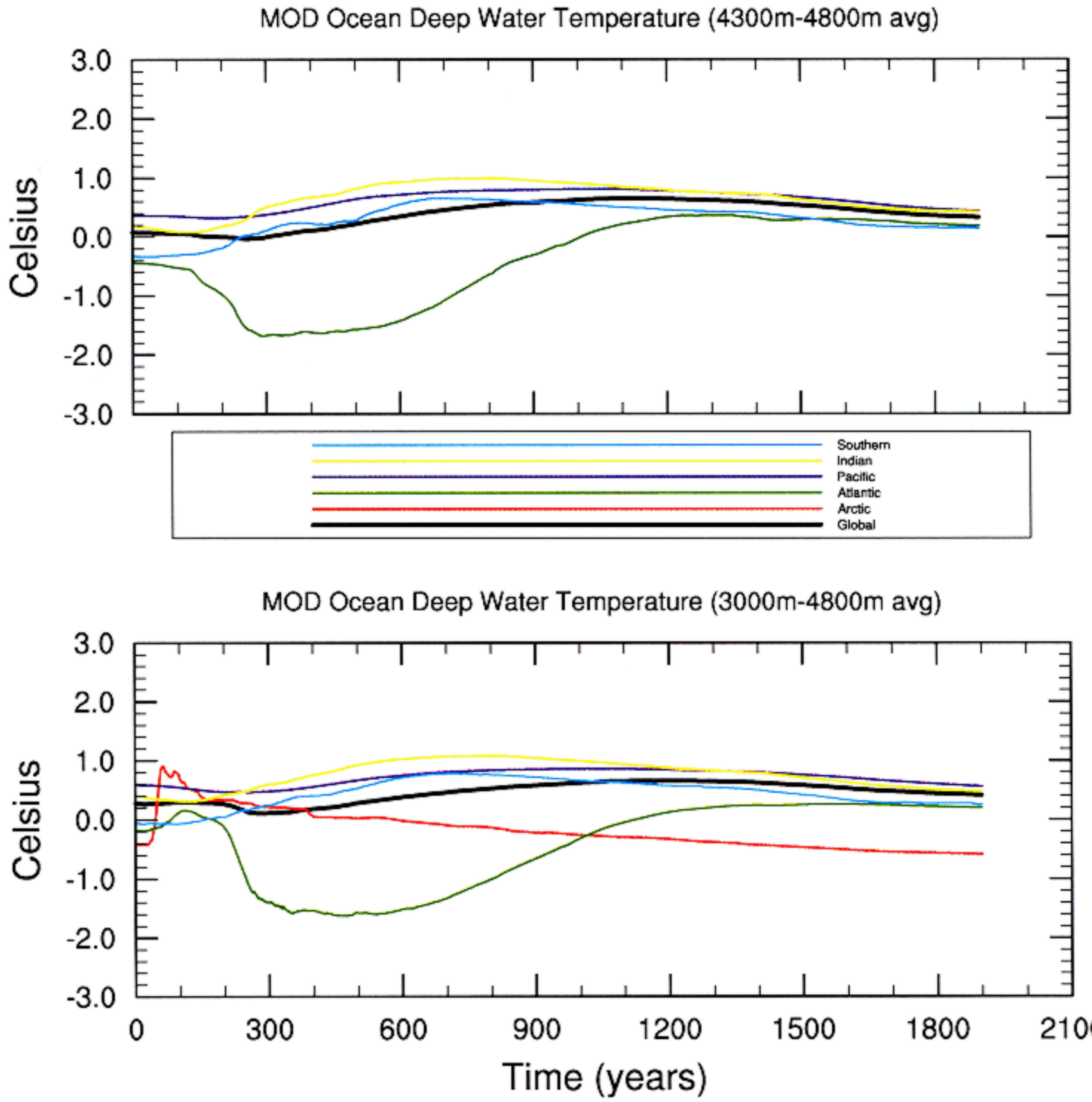

Fig. 6. Spin-up to equilibrium of the deep water temperatures in each of the ocean basins in the modern control integration.

which NADW penetrates. Under modern climate conditions, the strength of the Atlantic overturning circulation is predicted to be approximately 22 Sv whereas under LGM conditions it is predicted to be approximately 12 Sv.

Insofar as the depth extent of the Atlantic overturning cell in the modern control model is concerned, this extends to a depth of approximately 2 km, whereas in the LGM simulation it extends only to a depth of approximately 1 km. Also evident in this figure is the fact that Antarctic Bottom Water extends much further northwards into the Atlantic Basin under LGM conditions as opposed to modern conditions. This is a clear example of the northern hemisphere–southern hemisphere "see-saw" upon which Broecker (e.g. 1998) has commented in connection with the apparently out-of-phase relationship of the expression of the Younger-Dryas event in Greenland and Antarctic ice cores. Blunier et al. (1998) have also discussed this phenomenon in connection with the Dansgaard–Oeschger cycles of Oxygen Isotope Stage 3. When deep water production near the pole in one hemisphere is reduced, for whatever reason, deepwater production near the pole in the opposite hemisphere is enhanced. Seidov et al. (2001) discuss in some detail the issue of the differential fresh water flux that is required to shut down NADW production as opposed to the lower amount that is required to shut down AABW production. Further analyses of the see-saw effect have also been discussed by Seidov and Maslin (2001). Weaver et al. (2003) have recently developed an argument, based upon this effect, which suggests that if meltwater pulse 1a revealed in Fairbanks (1989) sea level record from Barbados were sourced from Antarctica, this might explain the onset of the Bolling warm period in the northern hemisphere. A discussion of the plausibility of this "see-saw scenario" will be found in Peltier (2003b).

Since the process of deep water production warms the overlying atmosphere, it is expected that Northern Hemisphere cooling would lead to Southern Hemisphere warming and vice-versa. It is interesting to compare these predictions concerning the variation of the THC in the Atlantic under glacial conditions to inferences of such changes based upon paleoceanographic measurements. Concerning the prediction that even the northernmost regions of the abyssal Atlantic should have

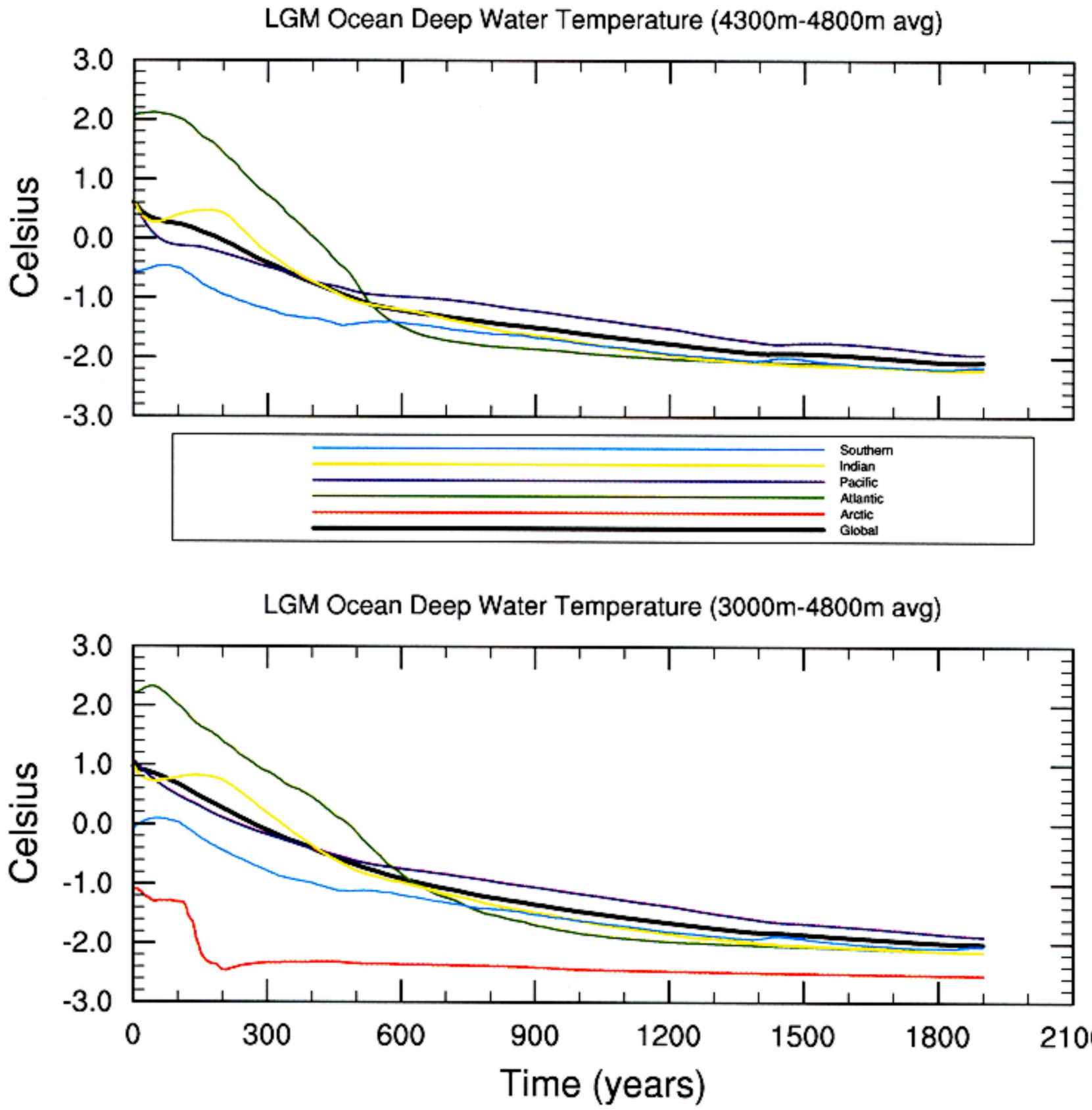

Fig. 7. Spin-up to equilibrium of the deep water temperature in each of the ocean basins in the LGM integration.

been inundated by Antarctic Bottom Water during the LGM, it has been clear for some time that this must have been the case based upon measurements of both passive tracer dispersal patterns (e.g. Boyle, 1992; Sarnthein et al., 1994; Duplessy et al., 1998) and of ^{14}C age differences between surface and deep water (Shackleton et al., 1988; Duplessy et al., 1989; Broecker et al., 1990; Adkins and Boyle, 1997) that this must have been the case. These analyses also provide clear support for the idea that the NADW driven cell became significantly shallower and weaker but was not entirely arrested under LGM conditions (see also Sarnthein et al., 1995; Seidov et al., 1996). Raymo et al. (1990) suggest that this same pattern of deep circulation variability was repeated in every glacial cycle of the Late Cenozoic for which sufficient information is available. Our simulation of the interior thermal and dynamical state of the LGM oceans is therefore in reasonably good accord with all of the proxy evidence available. This is in spite of the fact that no allowance has been made for any influence of the increase in mean salinity under glacial conditions and furthermore that no detailed analysis of the continental component of the hydrological cycle is accounted for. Water that is shed from the continents as run-off in the model we are employing is simply applied uniformly over the surface of the global ocean, no account therefore being taken of the fact that the discharge to the oceans actually occurs via a river network characterized by the existence of several extremely active discharge points at the mouths of major rivers and via a network of "ice streams" through which icebergs are continuously discharged from the great continental ice sheets. Based upon the success of the model which excludes these influences, we are inclined to believe that these additional sources of complexity must have only modest influence insofar as the LGM state of the climate system is concerned. This success furthermore suggests that the 1/3% increase of mean ocean salinity over the course of the model integrations, as documented in Fig. 5, may not be significantly biasing our results.

In considering the reason for the marked reduction in the strength of the Atlantic THC under LGM conditions, it proves useful to consider the nature of the sea

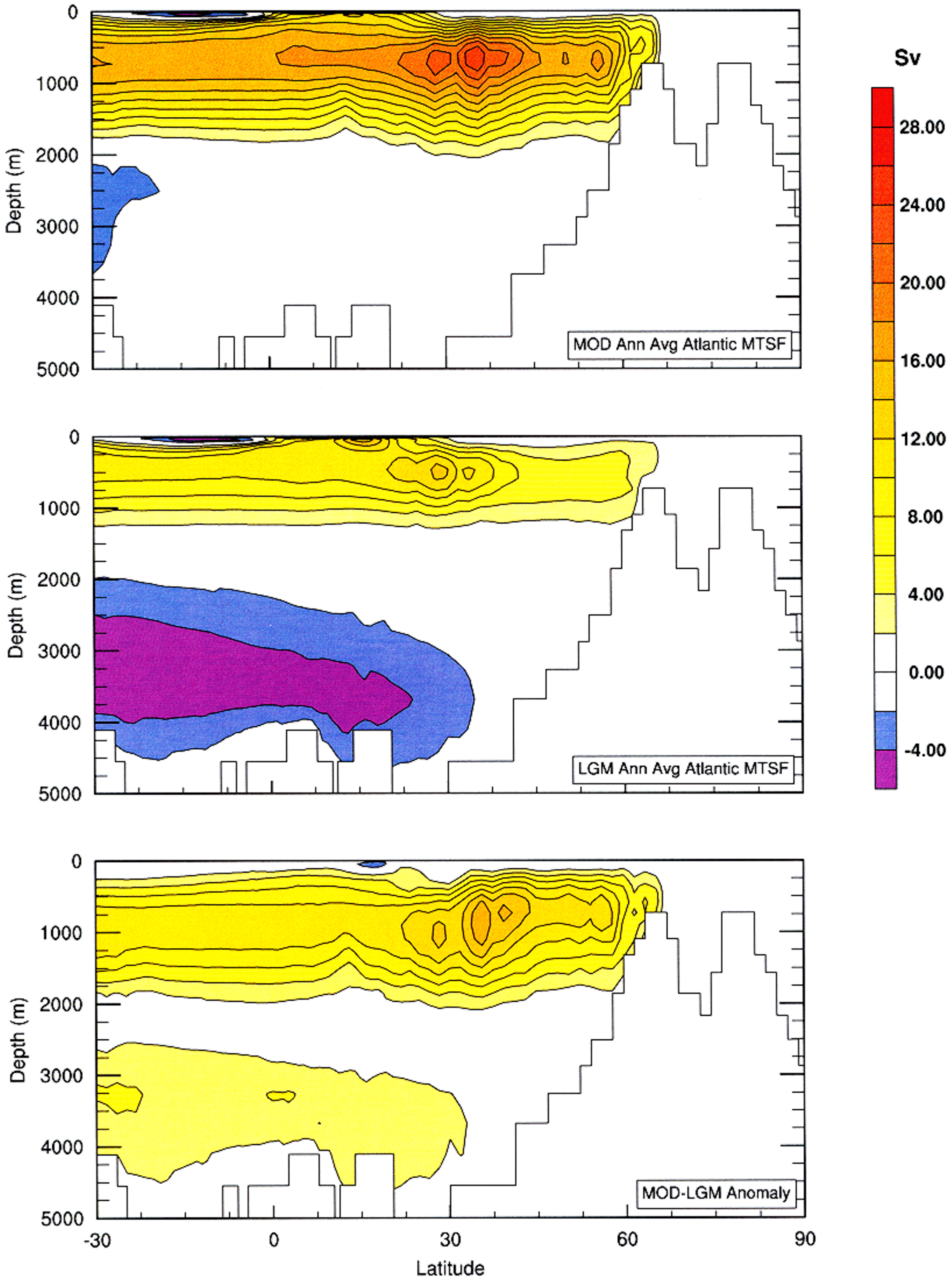

Fig. 8. The meridional transport streamfunction in the Atlantic basin between 30°S latitude and the north pole for both the modern and LGM integrations, as well as the difference between them. See the text for discussion.

ice distribution through the annual cycle at this time. Fig. 9 shows the month-by-month pattern of sea ice fraction predicted by the model in terms of the difference between the LGM and modern patterns. Obvious by inspection of these results is the fact that the concentration of sea ice under LGM conditions is strongly enhanced, with the southern boundary of essentially perennial sea ice markedly shifted to lower latitude. This shift in the pattern of sea ice variation through the annual cycle is such as to maintain essentially perennial ice cover over both of the primary regions in which NADW forms today, namely the GIN seas and the Labrador Sea. Recent analyses of the density variation through the water column in the

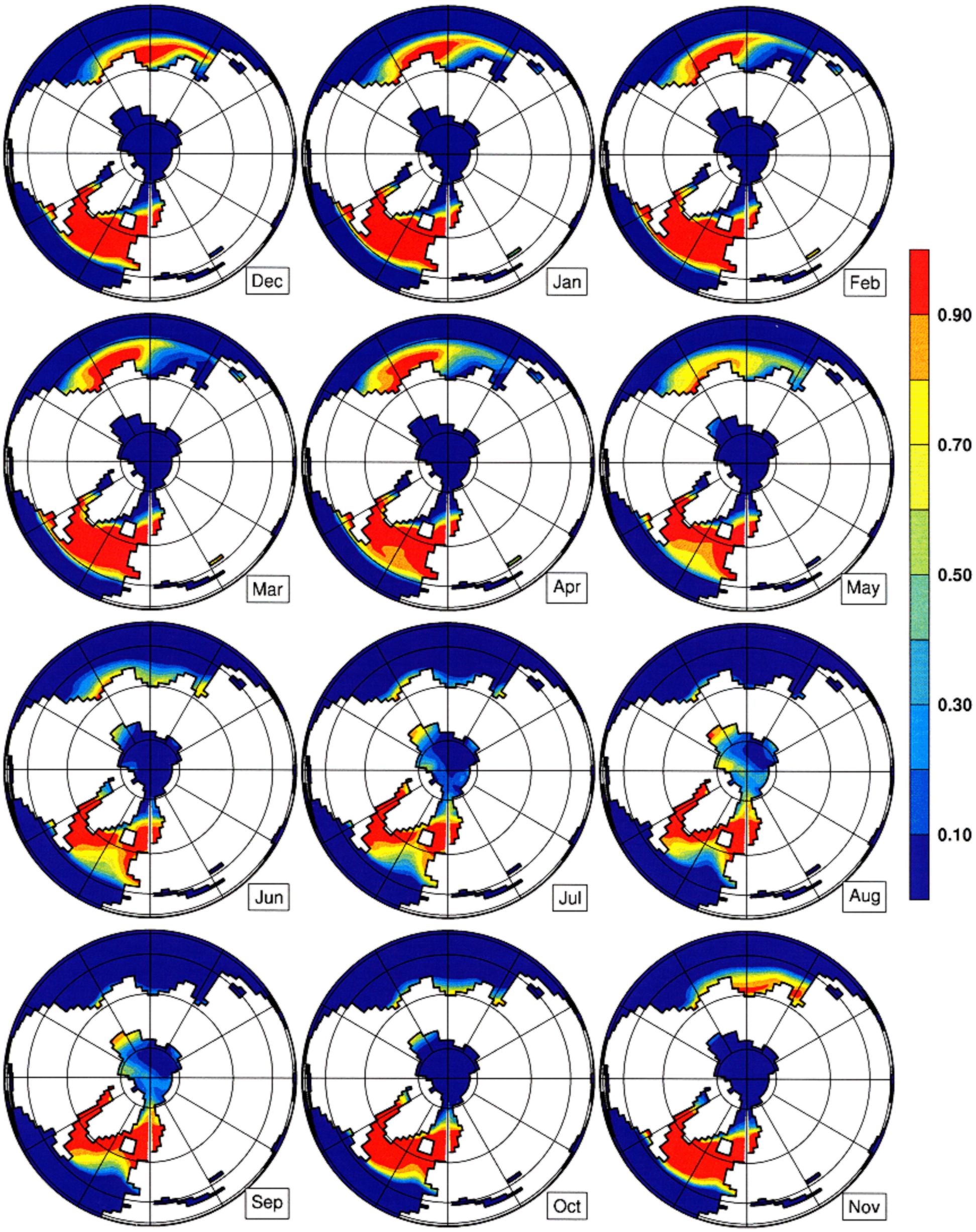

Fig. 9. Variation of the changing sea ice fraction over the annual cycle expressed as the difference between the LGM and modern control distributions.

Labrador Sea (de Vernal et al., 2002) have strongly suggested that the column was strongly stratified at LGM and therefore that this region of NADW formation was inactive at this time. Isotopic evidence has long supported the notion that the Norwegian sea also ceased to be a source of NADW under glacial conditions (Duplessy et al., 1975). The NADW that continues to be produced under LGM conditions forms primarily at the southern margin of sea ice advance where it is significantly influenced by the brine rejection process.

Since the first draft of this paper was written and submitted for publication, the interesting paper by Shin et al. (2003) has appeared in which the authors have

employed the same version of the CCSM that we are using to study LGM climate. They have also partly employed the ICE-4G (VM2) model of Peltier (1994, 1996) to fix the surface boundary conditions although they have not used this consistently by adopting both the land–sea mask and paleobathymetry that have been provided along with the paleotopography of the ice covered regions. Neither have they employed the implicit-ice correction described in Peltier (1998). The most significant difference between the Shin et al. (2003) simulation of LGM climate and that reported here, however, relates to the manner in which the models have been "spun-up" to statistical equilibrium. In Shin et al. (2003), the authors have sought to employ a less computationally expensive means of achieving equilibrium than the "brute-force" methodology we have elected to use in which the computation of LGM climate has been performed by integrating from the modern equilibrium solution in fully coupled mode for more than 2000 simulated calendar years. In Shin et al. (2003), in comparison, the authors have employed the deep water acceleration scheme of Bryan (1984) in an attempt to reach equilibrium in a more cost effective manner. Now it is well known that this procedure is not energy conserving. Furthermore, Peltier and Solheim (2001) have already compared its performance in the context of an initial analysis of the problem of LGM climate reconstruction and found it to deliver results that are significantly discrepant with those obtained by direct integration. A clear indication of the impact of this methodology upon the Shin et al. results for LGM climate concerns their result for the strength of the Atlantic THC, which in their Fig. 4 is shown to be approximately 20 Sv, essentially the same as modern and therefore distinctly at odds with the paleoceanographic inferences discussed previously. It seems clear to us that one should not employ the deep water acceleration scheme in an effort to save CPU time, since the price in terms of accuracy is far too high.

Similarly notable as the recent paper of Shin et al. (2003) and those of Hewitt et al. (2001, 2003) is the paper of Kim et al. (2003) in which the authors employed the second generation Canadian Centre for Climate modelling and analysis (CCCma) coupled general circulation model (CGCM2), the primary components of which have been fully described in McFarlane et al. (1992), Flato et al. (2000) and Boer et al. (2000). Similar to the NCAR paleoclimate version of the CCSM that we are employing in the present paper, this model is also based upon a T32 atmospheric spectral model but an ocean model with $1.875° \times 1.875°$ horizontal resolution, somewhat higher resolution than the $3° \times 3°$ ocean module in the paleoclimate version of the NCAR CCSM. The results obtained for the LGM climate in this model are characterized by a decrease of approximately 10°C in global mean surface air temperature (compared with the 9°C decrease we have obtained using the CCSM). The decease of global SST obtained in this analysis was 5.6°C (compared with the 4°C decrease delivered by the CCSM). In the tropics, the Kim et al. analyses delivered a cooling of SSTs of 6.5°C (compared to the 4.5°C value delivered by the CCSM). The reduction in global mean precipitation was 15%, close to the 19% drop obtained using the CCSM. The results delivered by this simulation for the Atlantic overturning circulation, however, are extremely poor. In the control model, the THC strength, at 12 Sv, is significantly weaker than observed. For the LGM (see their Fig. 18), there is essentially no NADW production at all, only a weak cell confined above 900 m depth but extending no further south than 30°N latitude, in marked contrast to the result delivered by the CCSM (see our Fig. 8) which agrees so well with the paleoceanographic proxy constraints. It is notable that this simulation, as with that of Shin et al. (2003), also employed a complex acceleration scheme in the attempt to speed up the approach to equilibrium. Our contention is that, as with the scheme of Bryan (1984), this is quite likely to strongly and adversely influence the results.

3.2. ENSO and tropical atmosphere–ocean interactions at LGM

Shifting focus now, from aspects of the mean state of the climate system at LGM, to its most prominent mode of internal variability, namely ENSO, it will prove useful to begin by considering the LGM equatorial ocean and especially its Pacific sector. Fig. 10 is especially useful in this regard as it shows the statistical equilibrium distribution of SST, from both modern and LGM integrations, in which the temperature fields displayed are annual averages. Inspection of the results shown in this figure demonstrates that tropical equatorial SSTs over the Pacific ocean are predicted to have been considerably colder than present, by an amount that exceeds 5°C over a narrow strip centred over the equator itself. The zonally averaged SST anomaly over the entire latitude range from 30°S to 30°N is, on average, near −4.5°C. Returning to the discussion of tropical SSTs provided in the Introduction of this paper, it will be clear that this value for the LGM depression of tropical SSTs lies approximately midway between the ~ -2°C value delivered by the alkenone proxy and the ~ -6°C value based upon isotopic measurements on corals and is in quite close accord with the most recent evidence based upon isotopic measurements on foraminifera from the Indo-Pacific warm pool (Visser et al., 2003). This would imply, taking the result from our model at face value, that the alkenones are underestimating and the corals overestimating the LGM SST depression in the tropics. In any event it is clear that the degree of cooling predicted by this model

is very much larger than was inferred by the CLIMAP collaboration based upon the use of a transfer function derived from species abundances of planktic foraminifera. Our results are also in reasonable accord with those of Bush and Philander (1998) whose analysis ignored the role of the THC in the phenomenon entirely. It should be noted that in Peltier and Solheim (2002), in which analyses were based upon results obtained after only the first 1000 years of spin-up, we obtained a tropical SST depression of only 2.5°C when the LGM result was compared to modern observations. It is important to recognize, however, that in that paper our comparison of the results of the LGM simulation to modern climate was not based upon a model–model intercomparisons, as at the time of writing this preliminary discussion we had yet to complete a new modern control integration for the ENSO resolving version of the lower resolution CCSM. Our intercomparisons in that paper were

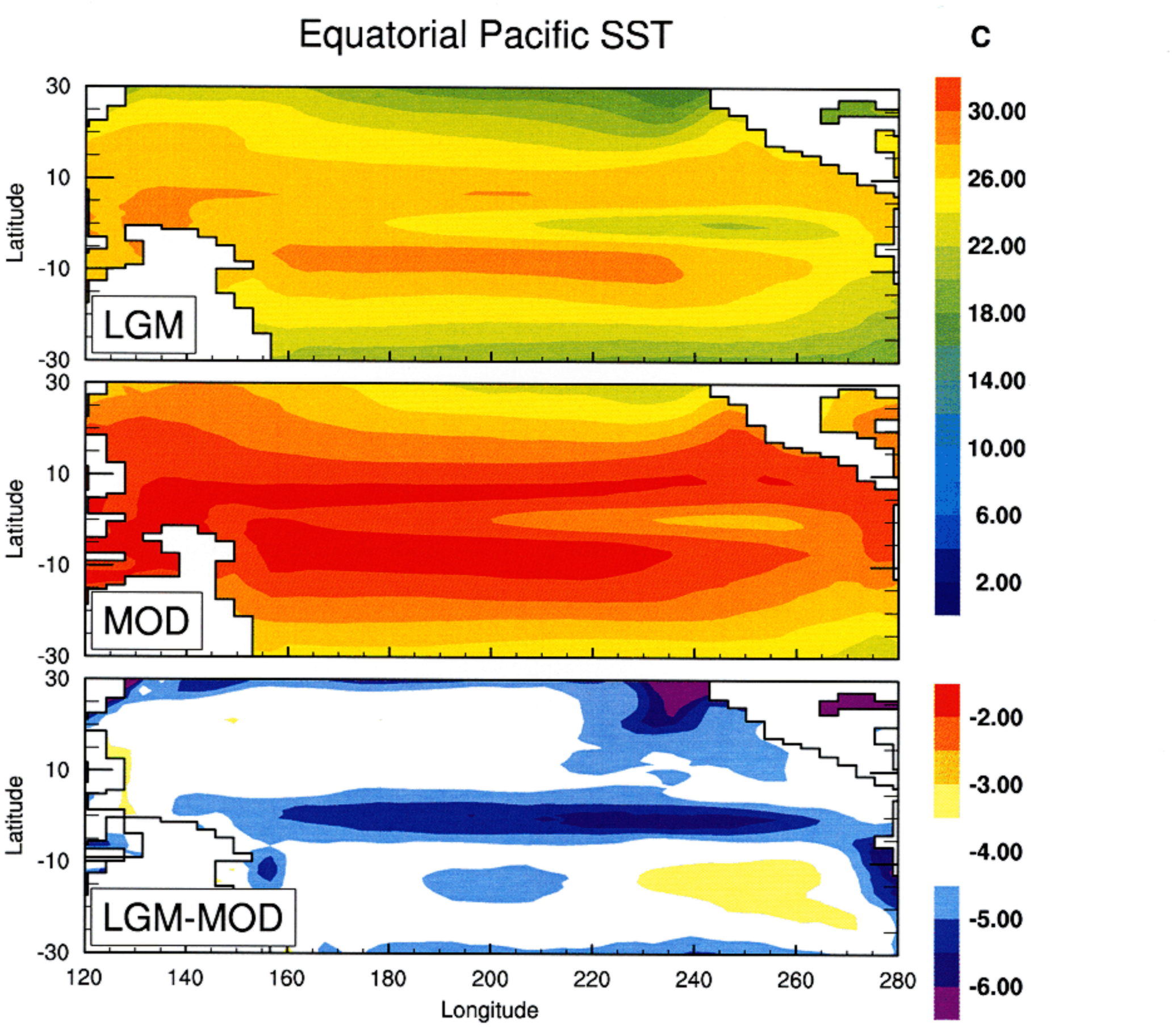

Fig. 10. Statistical equilibrium distributions of modern control and LGM distributions of sea surface temperatural over the equatorial Pacific Ocean, as well as the difference between them expressed as a latitude dependent zonal average.

therefore based upon a comparison of the results from the LGM integration with modern observations. This explains the discrepancy between the preliminary result in Peltier and Solheim (2002) and that reported here based upon statistical equilibrium model results for both modern and LGM climate. (The interested reader should note that the caption to Fig. 5 of Peltier and Solheim (2002) is misleading in this regard).

Because the model we are employing in the analysis of LGM climate is one that resolves the ENSO phenomenon, it is clearly interesting to employ it to estimate the changes in this process that should have accompanied glacial conditions. Because our coupled atmosphere–ocean model has been integrated over such an extended period of time, we are clearly in a position to construct a "composite" El Niño, as well as a composite La Niña, by stacking and averaging over a large number of such events based upon the application of some strength cut-off to an appropriate index of the phenomenon as a means of selecting those "events" which will be allowed to contribute to the composite. For the construction of the composite ENSO event that we will discuss herein, we have stacked all El Niño (and La Niña) events in which the amplitude of the equatorial southern oscillation index (EQSOI) is more than 1.5 standard deviations above (below) the mean. The respective composites have been formed by all events that satisfied this criterion over the final 200 years of both the modern control and LGM integrations and are shown in Figs. 11 and 12 respectively. The composite indices shown in these figures, for the EQSOI (normalized sea level pressure difference between Darwin and Tahiti), Nino3 (SST in the cold tongue), Nino4 (SST in the warm pool) and Nino1 + 2 (SST in the region of upwelling along the west coast of S. America) have been produced on the basis of averaged stacks extending 2.5 years prior to the event in question and 2.5 years after. Inspection of these composites will show that they are almost precisely symmetric between El Niño and La Niña. Furthermore, there is little evidence in them of any significant change in the amplitude of individual events of either parity although the LGM strength of the Nino3 index is

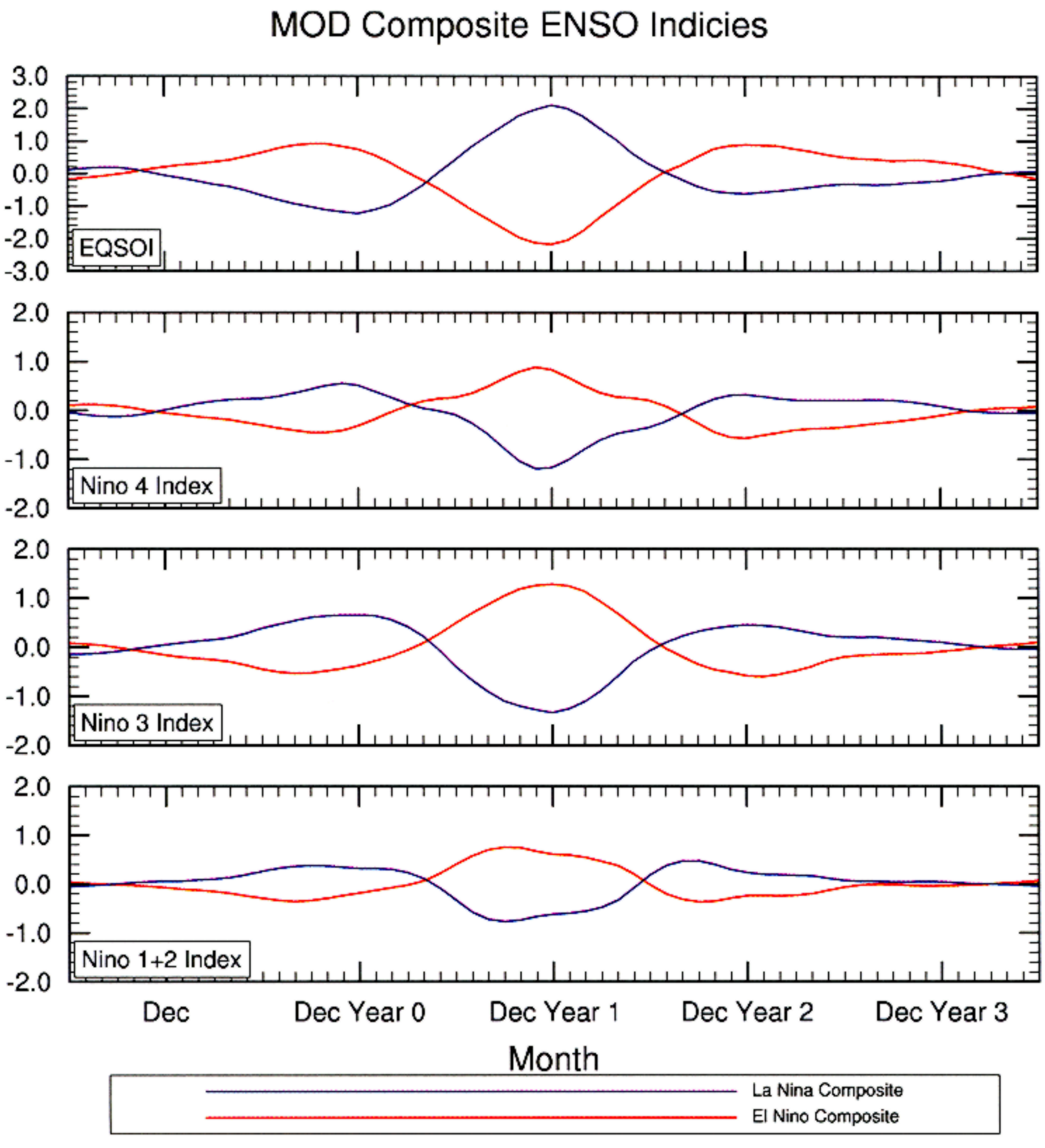

Fig. 11. ENSO indices for the composite El Niño and La Niña under modern climate conditions.

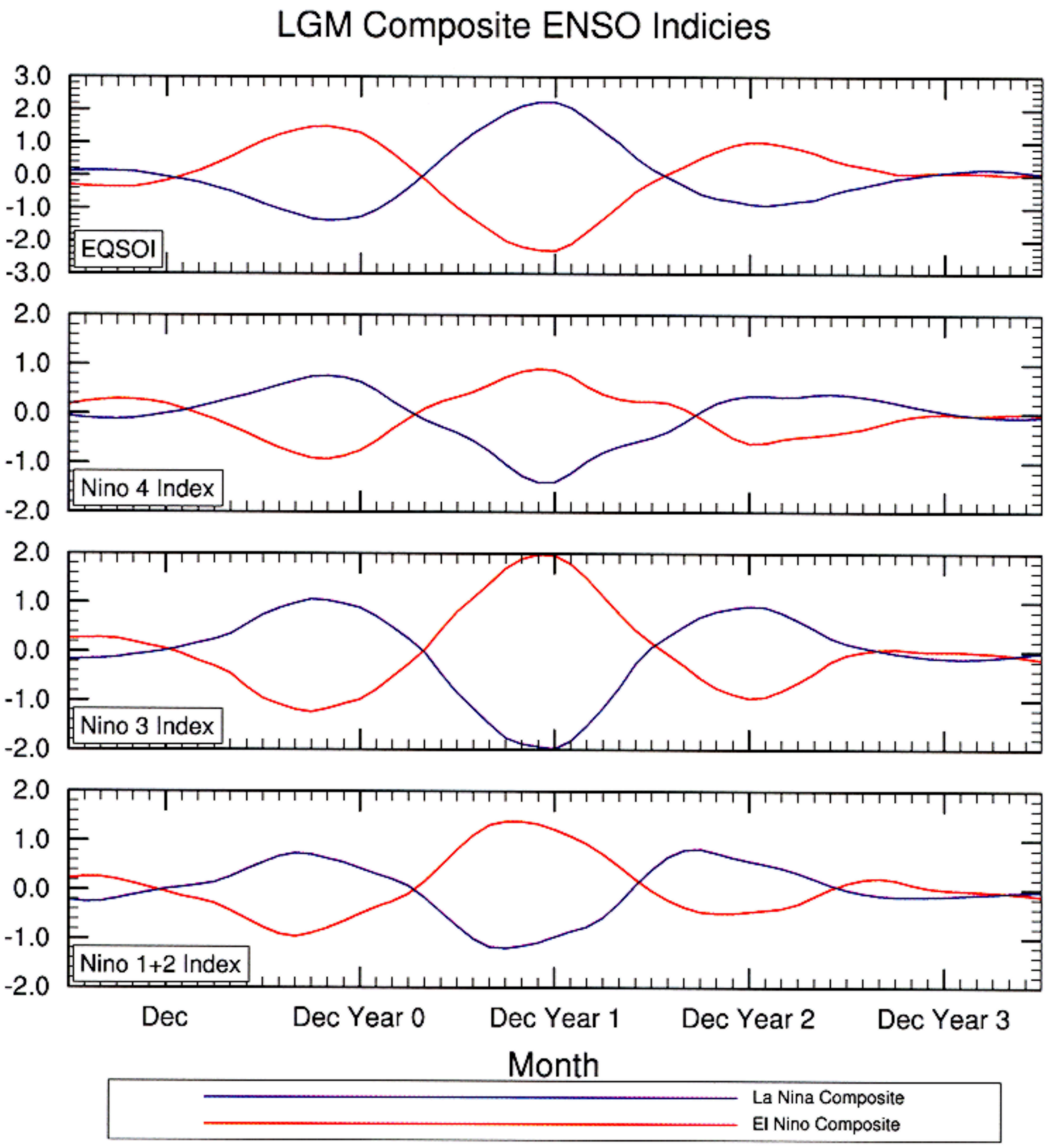

Fig. 12. ENSO indices for the composite El Niño and La Niña under LGM conditions.

approximately 25% stronger than its strength in the modern integration. Since this index is based upon the SSTs characteristic of the cold tongue (see e.g., Philander, 1990, for a good discussion of the ENSO indices that we are discussing herein), the implication is that ENSO was somewhat more intense in the glacial period that it is under modern climate conditions. It is important to understand, however, that these ENSO indices have been constructed using data from which the annual cycle has been removed, and this means that such composite indices do not provide a reliable measure of relative intensity.

A clearer measure of the relative intensity of variability between the LGM and modern simulations is provided by intercomparison of the variance through the annual cycle of SST in the Nino3 region. This intercomparison is shown in Figs. 13a and b, inspection of which demonstrates the marked increase of SST variability between the modern and LGM runs of the model in the Pacific cold tongue on the equator. Further support for the validity of this conclusion is shown in Fig. 14, where we compare the power spectra for the various ENSO indices between the modern and LGM integrations. Although the power spectra for the EQSOI indicates no significant change from modern to LGM, it is quite clear on the basis of the spectra shown for the other ENSO indices that the ENSO phenomenon is expected to have been more powerful under glacial conditions than it is under modern conditions, a result that is consistent with the preliminary analyses discussed in Peltier and Solheim (2002), analyses that were conducted when only 1000 years of the integration to statistical equilibrium had been completed. Notable also by inspection of Fig. 14 is the fact that the model predicts no significant shift in the frequency of El Niño events although there is somewhat more power at lower frequency under glacial conditions.

Although there have not been a large number of attempts to infer the strength of the ENSO phenomenon under climate conditions that differ markedly from the

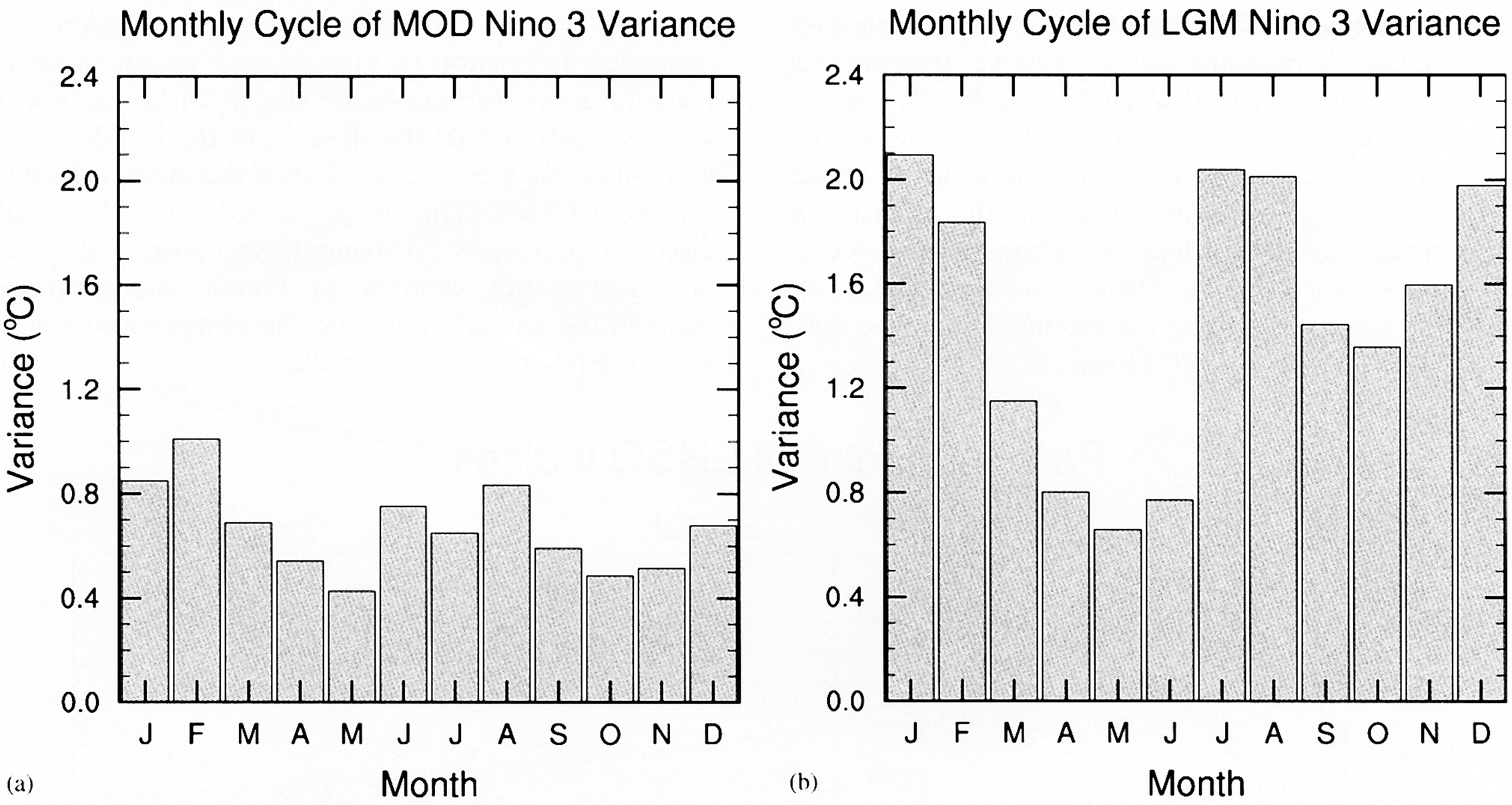

Fig. 13. SST variance in the Nino3 region (cold tongue) over the annual cycle from both the modern control (a) and LGM (b) integrations.

present, on the basis of either models or paleoclimatological proxy measurements, some efforts of this kind have been conducted. For example, Cane (1998) and Clement et al. (1999) have employed the "anomaly" based Cane–Zebiak model to investigate the way in which the strength of ENSO might be expected to change as a consequence of variations in orbital forcing. A further theoretical analysis, by Federov and Philander (2000), focused upon the question as to whether ENSO is amplifying under modern greenhouse warming conditions, and more generally commented upon the question as to how changes in mean climate state are expected to impact the strength of the phenomenon. In terms of efforts based upon the use of paleodata to directly infer the temporal variability of ENSO through time, the paper by Tudhope et al. (2001) is probably the most detailed. These authors employed $\delta^{18}O$ measurements on fossil corals from the Papua, New Guinea sequences to investigate the strength of the variability in an ENSO spectral band pass between periods of 2.5 and 7 years. Their analysis delivered a marked decrease of ENSO strength in the mid-Holocene warm period at 6.5 ka (see their Fig. 4) relative to modern, such that the mid-Holocene amplitude is approximately 1/3 of the modern amplitude. Although their results do not include estimates for ENSO strength in the interval between 6.5 ka and 38 ka that includes the LGM, their results for Marine Oxygen Isotope Stage 3 (MOIS3) of the glacial period suggest that the amplitude of ENSO during this period was no more than half the modern amplitude. Since this period was punctuated by the Dansgaard-Oeschger and Heinrich event phenomena (see Hemming, 2003 for a recent review), however, it is probably not reasonable to imagine that ENSO during this period would have been similar in any way to ENSO at LGM, a period that was free of the intense millennium timescale variability that was characteristic of OIS3. Although our result, that ENSO is expected to have been stronger at LGM than it is at present, seems to be inconsistent with the conclusions of Tudhope et al. (2001), it does appear to be somewhat more consistent with the results reported by Clement et al. (1999), obtained using the Cane–Zebiak "anomaly" based model in which the only influence included was that due to variable orbital forcing. However, this model appears to predict maximum El Niño amplitude during deglaciation rather than at LGM. Since we have not attempted to reconstruct ENSO during the period of active deglaciation using the full coupled model being employed herein, we are in no position to comment as to whether we would or would not agree with the Clement et al. prediction based on orbital forcing alone.

Further insight into the nature of the enhanced ENSO that our model is predicting for the LGM is provided in Figs. 15 and 16 where we illustrate the composite El Niño, for modern and LGM respectively, in terms of the time-dependent temperature anomaly in the upper ocean. The data shown in these figures, on the depth-longitude plane across the Pacific, consist of ocean temperature averaged over the slab extending from 2°S latitude to 2°N latitude. Inspection of these figures will

demonstrate that El Niño begins with the appearance on the tropical thermocline of a positive temperature anomaly in the west central equatorial Pacific Ocean. This anomaly is produced by a depression of the thermocline forced by an atmospherically induced convergence of ocean water towards the equator, a convergence driven by a localized atmospheric circulation anomaly (not shown). Once formed, this anomaly thereafter propagates along the thermocline to the east, finally erupting as a full blown El Niño once the anomaly reaches the west coast of the S. American continent. Inspection of Figs. 15 and 16, on which the temperature perturbations are shown on the same scale, will demonstrate that the strength of the LGM El Niño is significantly greater than that of the modern El Niño (in the CCSM). This is in accord with the results discussed previously involving the composite indices, the month-by-month changes in Nino3 index variance through the annual cycle, and the power spectra of the various ENSO indices themselves.

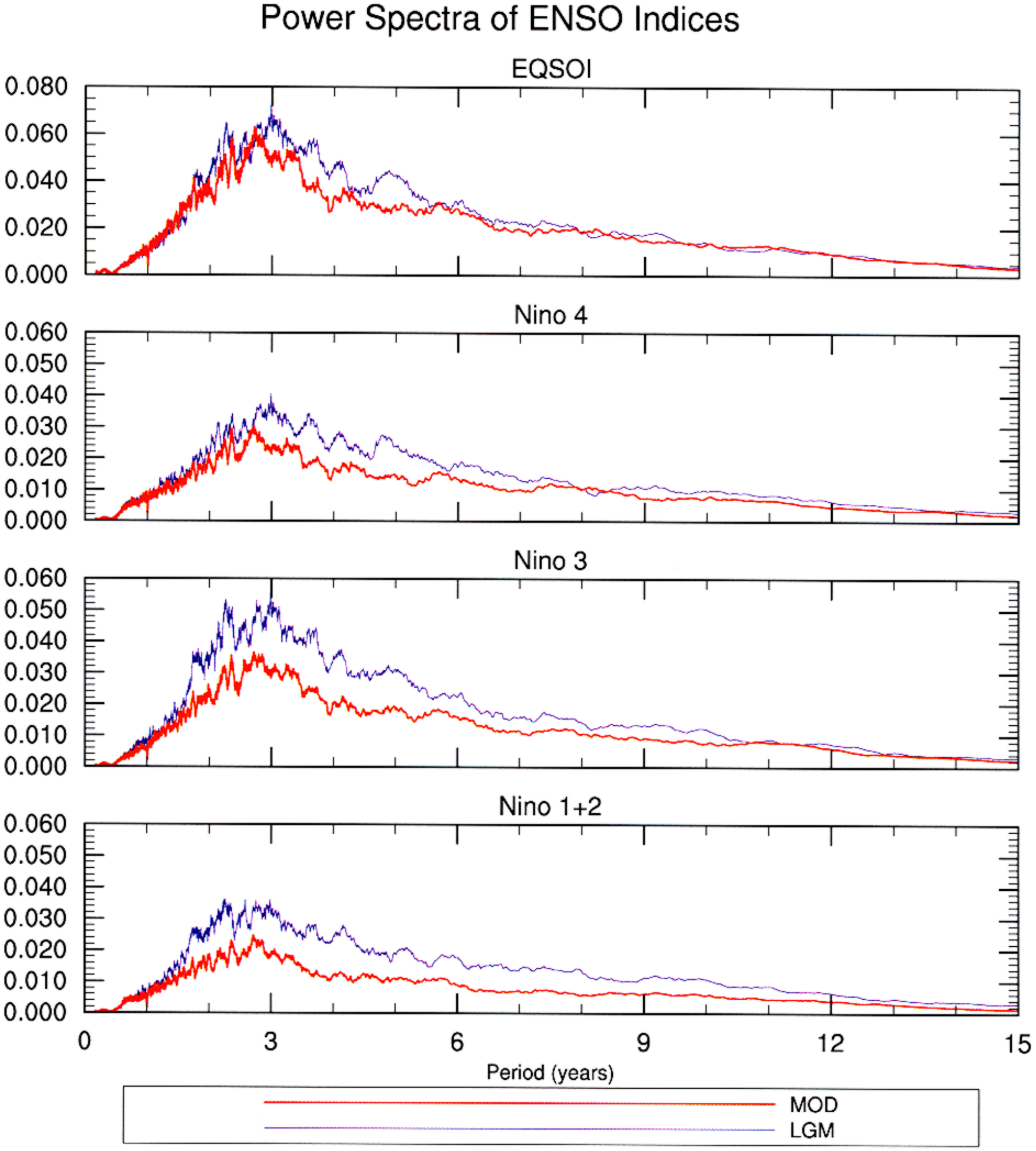

Fig. 14. Power spectra of the ENSO indices (as a function of power expressed as a function of period) for both the modern control and LGM integrations. Although there is no significant shift in the dominant period of the phenomenon, which is near 3 years in the CCSM, there is a significant increase in the strength of El Niño under ice-age conditions.

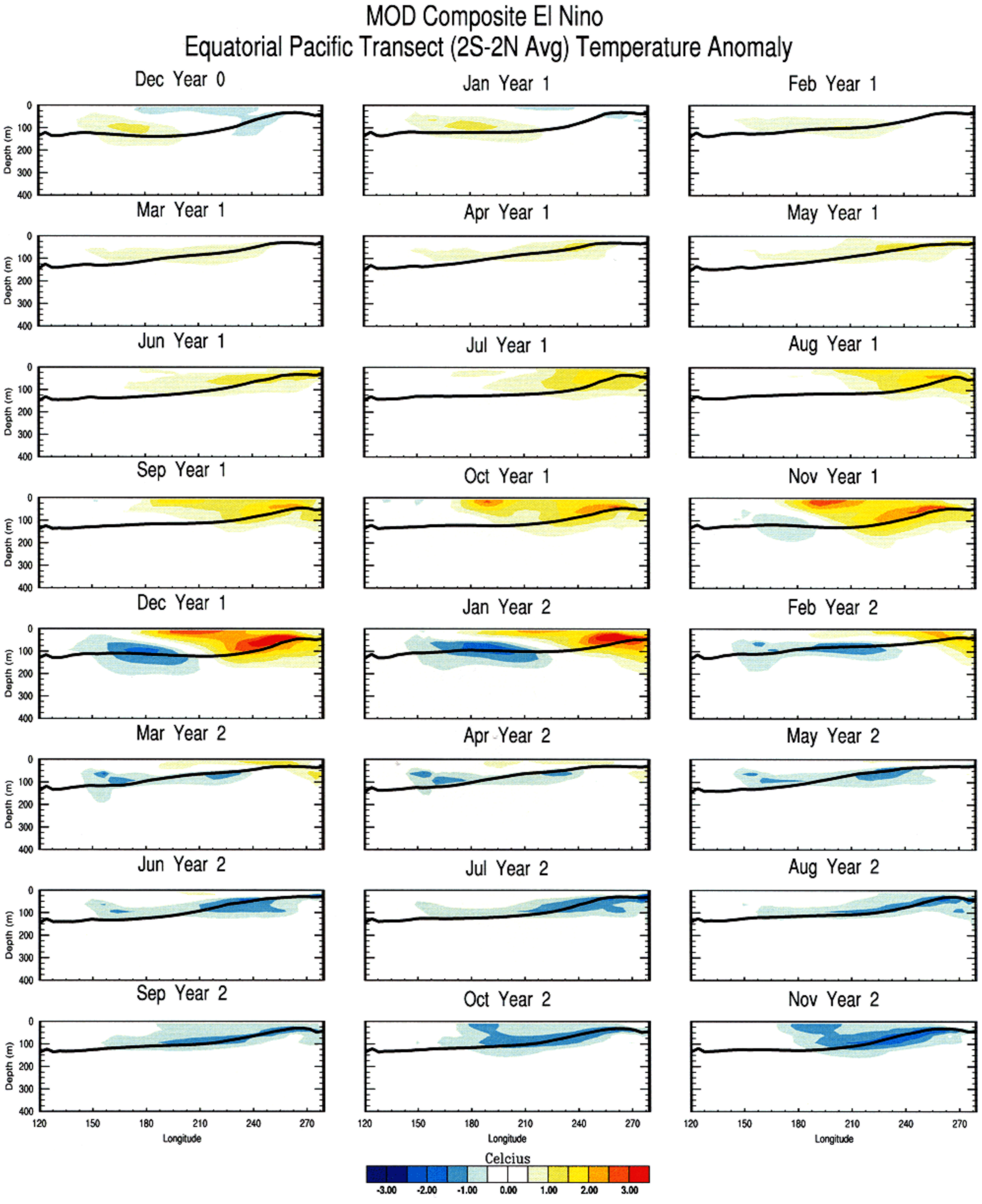

Fig. 15. The composite El Niño in the modern control integration expressed in terms of the temperature of the upper ocean averaged in latitude over the range from 2°S latitude to 2°N latitude. The composite is constructed by month from 1 year prior to the "event" to 1 year after the event. Evident by inspection of the composite is the appearance of the warm anomaly on the equatorial thermocline in the west central Pacific and its propagation thereafter to the east. Full-blown El Niño conditions develop upon the arrival of this eastward propagating anomaly at the west coast of the South American continent.

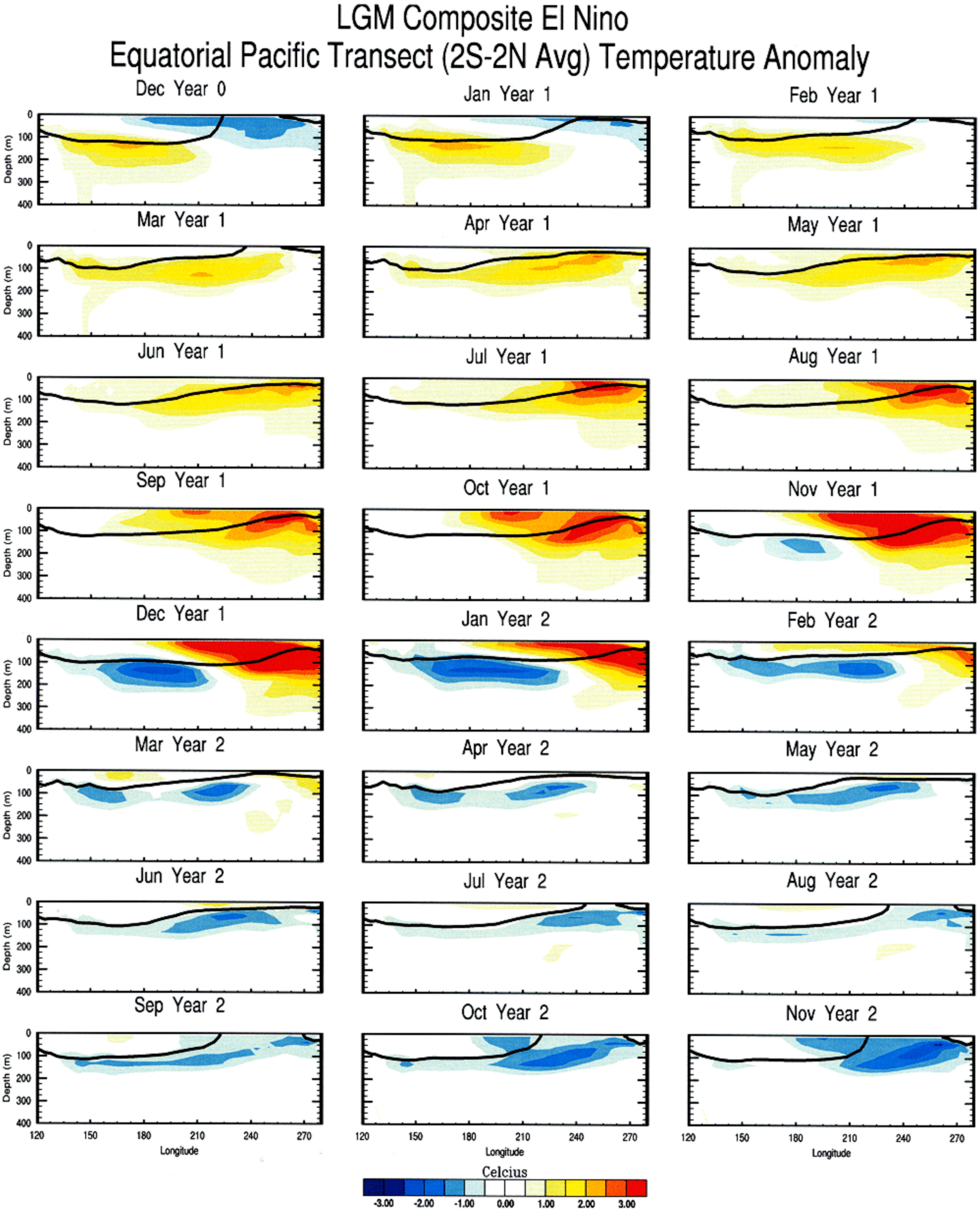

Fig. 16. Same as for Fig. 14 but from the LGM integration.

4. Conclusions

In this paper we have focused upon several of the expected characteristics of the climate system at LGM, based upon simulations conducted using the Community Climate System Model of the NCAR. Our intercomparisons of statistical equilibrium results for LGM and modern climate that were derived from

integrations of approximately 2 kyrs duration, suggest several tentative conclusions, many of which are in close accord with paleoceanographic inferences. First, concerning the mean climate state at LGM, our results suggest that tropical SSTs were depressed on average by approximately 4.5°C at that time and that the temperatures of the abyssal oceans were approximately −2°C. Insofar as the Atlantic overturning circulation is concerned, our results suggest that the cell driven by NADW production was significantly shallower and significantly weaker at LGM (~12 Sv) than it is under modern conditions (~22 Sv), a result that is an excellent accord with paleoceanographic inferences. Secondly, concerning the ENSO mode of interannual variability, our results very strongly suggest that El Niño was considerably more intense under full glacial conditions.

Aside from these primary results of the CCSM integrations for LGM climate that have been described herein, the implications of the result concerning the tropical depression of SST may be rather important—and so perhaps deserves special comment. Bacastow (1996) has provided rather convincing evidence that a tropical SST cooling of order 5°C may be expected to lead directly, through the temperature dependence of the solubility of CO_2 in sea water, to a decrease in atmospheric CO_2 concentration of approximately 50 ppmv. This is more than 60% of the observed decrease of 80 ppmv that occurred during the transition to glacial conditions. This suggests that further analysis of the relative importance of the solubility pump and the biological pump may be warranted. Also in connection with this fundamental issue of the LGM carbon cycle, it may be of considerable importance to recognize the connection between the ability of the ocean to draw-down CO_2 from the atmosphere and wind strengths over the ocean basins. Because the "piston velocity" depends upon the cube of the wind-speed and because this further multiplies solubility in the expression for the magnitude of air–sea gas exchange, the fact that LGM wind speeds over the oceans are considerably higher than modern and their variability more intense (e.g. El Niño), will also contribute to an enhancement of the solubility effect under LGM conditions. Detailed further discussion of the implications of the results reported herein concerning the glacial carbon cycle will be presented elsewhere.

The data sets that have been generated in the course of this work are expected to provide a basis for several further analyses of the differences in climate that existed between LGM and modern conditions. A detailed intercomparison of the atmospheric circulations between these two epochs of time is certainly warranted as is the examination of the primary modes of polar climate variability, in particular the North Atlantic oscillation/Arctic oscillation and the northern hemisphere and southern hemisphere annular modes. In the northern hemisphere in particular, we expect that the impact of the presence of the Laurentide ice-sheet upon the mid-latitude tropospheric jet stream position will be severe. Storm track positions will thereby be strongly influenced and through this effect the delivery of moisture to the ice complexes themselves. Accurate analyses of the influence of the ice-sheets upon these characteristics of the atmospheric general circulation will require use of the new ICE-5G reconstruction of the topographies of the glaciated continents that is currently under construction (see Peltier 2002c, 2003a for recent discussions). In further work to be discussed elsewhere, we will describe the impact upon the atmospheric and oceanographic general circulations of these required modifications to the paleotopography and land–sea mask embodied in the ICE-4G model that has been employed herein.

References

Adkins, J.F., Boyle, E.A., 1997. Changing atmospheric $\delta^{14}C$ and the record of deep water paleo-ventilation ages. Paleoceanography 12, 337–344.

Adkins, J.F., McIntyre, K., Schrag, D., 2002. The salinity, temperature, and $\delta^{18}O$ of the glacial deep ocean. Science 298, 1769–1773.

Bacastow, R.B., 1996. The effect of temperature change of the warm surface waters of the oceans on atmospheric CO_2. Global Biogeochemical Cycles 10, 319–333.

Bard, E., Rostek, F., Sorizongi, C., 1997. Interhemispheric synchrony of the last deglaciation inferred from alkenone paleothermometry. Nature 385, 707–710.

Blunier, T., et al., 1998. Asynchrony of the Antarctic and Greenland climate change during the last glacial period. Nature 394, 739–743.

Boer, G.J., Flato, G.M., Reader, M.C., Ramsden, D., 2000. A transient climate change simulation with greenhouse gas and aerosol forcing: experimental design and comparison with the instrumental record from the 20th Century. Climate Dynamics 16, 405–425.

Boville, B.A., Gent, P., 1998. The NCAR climate system model, version 1. Journal of Climate 11, 1115–1130.

Boyle, E.A., 1992. Cadmium and $\delta^{13}C$ paleochemical ocean distributions during the stage 2 glacial maximum. Annual Review of Earth and Planetary Science 20, 245–287.

Boyle, E., 2002. Oceanic salt switch. Science 298, 1724–1725.

Broecker, W.S., 1998. Paleocean circulation during the last deglaciation: a bipolar sea-saw? Paleoceanography 13, 119–121.

Broecker, W.S., Denton, G.H., 1990. The role of atmosphere–ocean reorganizations in glacial cycles. Geochimica et Cosmochimica Acta 53, 2465–2501.

Broecker, W.S., Hung, T.H., Trumbore, S., Bonani, G., Wolfli, W., 1990. The distribution of radiocarbon in the glacial ocean. Global Biogeochemical Cycles 4, 103–117.

Bryan, K., 1984. Accelerating the convergence to equilibrium of ocean-climate models. Journal of Physical Oceanography 14, 666–673.

Bush, A.B.G., Philander, S.G.H., 1998. The role of ocean–atmosphere interactions in tropical cooling during the Last Glacial Maximum. Science 279, 1341–1344.

Cane, M.A., 1998. A role for the tropical Pacific. Science 282, 59–61.

Clement, A.C., Seager, R., Cane, M.A., 1999. Orbital controls on the El Niño/Southern Oscillation and the tropical climate. Paleoceanography 14, 441–456.

CLIMAP Project Members, 1976. The surface of the ice-age earth. Science 191, 1131–1137.

CLIMAP Project Members, 1981. Seasonal reconstructions of the Earth's surface at the Last Glacial Maximum. Geological Society of America Map Chart Service, MC-36.

CLIMAP Project Members, 1984. The last interglacial ocean. Quaternary Research 21, 123–224.

de Vernal, A., Hillaire-Marcel, C., Peltier, W.R., Weaver, A.J., 2002. The structure of the upper water column in the northwest North Atlantic. Paleoceanography 17(4), 2:1–2:15 (10.1029/2001 PA000665).

Duplessy, J.C., Chenouard, L., Vila, F., 1975. Weyl's theory of glaciation supported by isotopic study of Norwegian core K11. Science 188, 1208–1209.

Duplessy, J.C., et al., 1988. Deepwater source variations during the last climatic cycle and their impact on the global deep water circulation. Paleoceanography 3, 343–360.

Duplessy, J.C., Arnold, M., Bard, E., Juillet Leclerc, A., Kallel, N., Labeyrie, L., 1989. AMS-C-14 Study of transient events and of the ventilation rate of the Pacific Intermediate Water during the last deglaciation. Radiocarbon 31, 493–502.

Federov, A.V., Philander, S.G., 2000. Is El Niño Changing? Science 288, 1997–2002.

Flato, G.M., Boer, G.J., Lee, W.G., McFarlane, N.A., Ramsden, D., Reader, M.C., Weaver, A.J., 2000. The Canadian Climate Centre for Modelling and Analysis global coupled model and its climate. Climate Dynamics 16, 451–467.

Guildersen, T.P., Fairbanks, R.G., Rubenstone, J.L., 2001. Tropical Atlantic coral oxygen isotopes: glacial–interglacial sea surface temperatures and climate change. Marine Geology 172, 75–89.

Hemming, S.R., 2003. Heinrich events: massive Late Pleistocene detritus layers of the North Atlantic and their global climate imprint. Reviews of Geophysics, in press.

Hewitt, C.D., Brocolli, A.J., Mitchel, J.F.B., Stouffer, R.J., 2001. A coupled model study of the last glacial maximum: was part of the North Atlantic relatively warm? Geophysical Research Letters 28, 1571–1574.

Hewitt, C.D., Stouffer, R.J., Brocolli, A.J., Mitchell, J.F.B., Valdes, Paul J., 2003. The effect of ocean dynamics in a coupled GCM simulations of the Last Glacial Maximum. Climate Dynamics 20, 203–218.

Imbrie, J., Kipp, N.G., 1971. A new micropaleontological method for quantitative paleoclimatology: application to a Late Pleistocene Caribbean core. In: Turehian, K. (Ed.), Late Cenozoic Glacial Ages. Yale University Press, New Haven, pp. 71–181.

IPCC, 2001. Climate Change. The Scientific Basis. Cambridge University Press, Cambridge.

Kim, S.-J., Flato, G.M., Boer, G.J., 2003. A coupled climate model simulation of the Last Glacial Maximum. Part 2: Approach to equilibrium. Climate Dynamics 20, 635–661.

Lea, D., Pak, D., Spero, H., 2000. Climate impact of Late Quaternary Equatorial Pacific sea surface temperature variations. Science 289, 1719–1724.

McFarlane, N.A., Boer, G.J., Blanchet, J.-P., Lazarie, M., 1992. The Canadian climate centre second generation general circulation model and its equilibrium climate. Journal of Climate 5, 1013–1044.

Meehl, G.A., Arblaster, J.M., 1998. The Asian–Australian monsoon and El Niño–Southern Oscillation in the NCAR climate system model. Journal of Climate 11, 1356–1385.

Meehl, G.A., Gent, P.R., Arblaster, J.M., Otto-Bluesner, B.L., Brady, E.C., Craig, A., 2001. Factors that affect the amplitude of El Niño in global coupled climate models. Climate Dynamics 17, 515–526.

Millero, F.J., 1978. Freezing point of sea water. In: Eighth Report of the Joint Panel on Oceanographic Tables and Standards, UNESCO Technical Paper on Marine Science, No. 28, Annex 6, UNESCO, Paris.

Otto-Bliesner, B., Brady, E.C., 2001. Tropical pacific variability in the NCAR climate system model. Journal of Climate 14, 3587–3607.

Peltier, W.R., 1994. Ice age paleotopography. Science 265, 195–201.

Peltier, W.R., 1996. Mantle viscosity and ice-age ice-sheet topography. Science 273, 1359–1364.

Peltier, W.R., 1998. Implicit ice in the global theory of glacial isostatic adjustment. Geophysical Research Letters 25, 3955–3958.

Peltier, W.R., 2002a. On eustatic sea level history, Last Glacial Maximum to Holocene. Quaternary Science Reviews 21, 377–396.

Peltier, W.R., 2002b. Comments on the paper of Yokoyama et al. (2000) entitled "Timing of the Last Glacial Maximum from observed sea level minima". Quaternary Science Reviews 21, 409–414.

Peltier, W.R., 2002c. Global glacial isostatic adjustment: paleogeodetic and space-geodetic tests of the ICE-4G (VM2) model. Journal of Quaternary Science 17, 491–510.

Peltier, W.R., 2003a. Global glacial isostasy and the surface of the Ice-Age Earth: the ICE-5G VM model and GRACE. Annual Review of Earth and Planetary Science 32, 111–149.

Peltier, W.R., 2003b. On the hemispheric origins of meltwater pulse 1a. Quaternary Science Reviews, in press.

Peltier, W.R., Solheim, L.P., 2001. Ice in the climate system: paleoclimatological perspectives. In: Matsuno, T., Kida, H. (Eds.), Present and Future of Modeling Global Environmental Change. Terra Scientific Publishing Company, Tokyo, pp. 221–241.

Peltier, W.R., Solheim, L.P., 2002. Dynamics of the ice-age earth: solid mechanics and fluid mechanics. Journal of Physics IV France 12, Pr10-95–Pr10-104.

Petit, J.R., et al., 1999. Climate and atmospheric history of the past 420,000 years from the Vostock ice core, Antarctica. Nature 399, 429–436.

Philander, S.G., 1990. El Niño, La Niña, and the Southern Oscillation. Academic Press Inc., New York, 293pp.

Pinot, S., Ramstein, G., Harrison, S.P., Prentice, I.C., Guiot, J., Stute, M., Joussaume, S., 1999. Tropical paleoclimates at the Last Glacial Maximum: comparison of Paleoclimate Modeling Intercomparison Project (PMIP) simulations and paleodata. Climate Dynamics 15, 857–874.

Raymo, M.E., Ruddiman, W.F., Shackleton, N.I., Oppo, D.W., 1990. Evolution of Atlantic–Pacific $\delta^{13}C$ gradients over the last 2.5 m.y. Earth and Planetary Science Letters 97, 353–368.

Reader, M.C., Fung, I., McFarlane, N., 2000. Mineral aerosols: a comparison of the Last Glacial Maximum and preindustrial Holocene. Canadian Journal of Earth Science 37, 751–767.

Sarnthein, M., Winn, K., Jung, S.J.A., Duplessy, J.-C., Labeyrie, L., Erlenkeuser, H., Ganssen, G., 1994. Changes in the east Atlantic deep-water circulation of the last 30,000 years: eight time-slice reconstructions. Paleoceanography 9, 209–267.

Sarnthein, M.E., Jansen, M., Weinelt, M., Arnold, M., Duplessy, J.-C., Erlenkeusen, H., Flatoy, H., Johanessen, G., Johannessen, T., Jung, S., Koc, N., Labeyrie, L., Maslin, M., Plauffman, U., Schultz, H., 1995. Variations in Atlantic surface ocean plaeoceanography, 50–80 N: a time slice record of the last 30,000 years. Paleoceanography 10, 1063–1094.

Seidov, D., Maslin, M., 2001. Atlantic ocean heat piracy and the bipolar climate see-saw during Heinrich and Dansgaard Oeschger events. Journal Quaternary Science 16, 321–328.

Seidov, D., Sarnthein, M., Statteger, K., Prien, R., Weinelt, M., 1996. North Atlantic ocean circulation during the Last Glacial Maximum and subsequent meltwater event: a numerical model. Journal of Geophysical Research C101, 16305–16332.

Seidov, D., Barron, E., Haupt, B.J., 2001. Meltwater and the global ocean conveyor: northern versus southern connections. Global and Planetary Change 30, 257–270.

Shin, S.-I., Liu, Z., Otto-Bliesner, B., Brady, E.C., Kutzbach, J.E., Harrison, S.P., 2003. A simulation of the Last Glacial Maximum climate using the NCAR CCSM. Climate Dynamics 20, 127–151.

Tudhope, A.W., Chilcott, C.P., McCulloch, M.T., Cook, E.R., Chappell, J., Ellam, R.M., Lea, D.W., Lough, J.M., Schimmield, G.B., 2001. Variability in the El Niño–Southern oscillation through a glacial–interglacial cycle. Science 291, 1511–1517.

Vettoretti, G., Peltier, W.R., McFarlane, N., 2000. Global water balance and atmospheric water vapour transport at Last Glacial Maximum: climate simulations with the Canadian Climate Centre for Modelling and Analysis atmospheric general circulation model. Canadian Journal of Earth Sciences 37, 695–723.

Visser, K., Thunell, R., Stott, L., 2003. Magnitude and timing of temperature change in the Indo-Pacific warm pool during deglaciation. Nature 421, 152–155.

Weaver, A.J., Eby, M., Fanning, A.F., Wiebe, E.C., 1998. Simulated influence of carbon dioxide, orbital forcing and ice sheets on the climate of the Last Glacial Maximum. Nature 394, 847–853.

Weaver, A.J., Saenko, O.A., Clark, P.U., Mitrovica, J.X., 2003. Meltwater pulse 1a from Antarctica as a trigger of the Bölling–Allerød warm interval. Science 299, 1709–1713.